NASA TECHNICAL NOTE

NASA TN D-4448

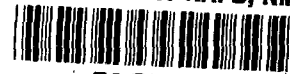$c.1$

NASA TN D-4448

LARGE-SCALE WIND-TUNNEL TESTS OF A DEFLECTED SLIPSTREAM STOL MODEL WITH WINGS OF VARIOUS ASPECT RATIOS

by V. Robert Page, Stanley O. Dickinson,
and Wallace H. Deckert

Ames Research Center
Moffett Field, Calif.

NATIONAL AERONAUTICS AND SPACE ADMINISTRATION • WASHINGTON, D. C. • MARCH 1968

LARGE-SCALE WIND-TUNNEL TESTS OF A DEFLECTED SLIPSTREAM

STOL MODEL WITH WINGS OF VARIOUS ASPECT RATIOS

By V. Robert Page, Stanley O. Dickinson,
and Wallace H. Deckert

Ames Research Center
Moffett Field, Calif.

LARGE-SCALE WIND-TUNNEL TESTS OF A DEFLECTED SLIPSTREAM

STOL MODEL WITH WINGS OF VARIOUS ASPECT RATIOS

By V. Robert Page, Stanley O. Dickinson,
and Wallace H. Deckert

Ames Research Center

SUMMARY

A wind-tunnel investigation was conducted to determine the longitudinal force characteristics of a large-scale model representative of a propeller-driven STOL transport aircraft. Longitudinal characteristics were obtained for a wing of aspect ratio of 5.7 that was fully immersed in the propeller slipstream and for wings of greater span (up to aspect ratio 8.1) that were only partially immersed in the propeller slipstream. Test configurations included: three wing spans, full-span leading-edge slats, full-span triple-slotted trailing-edge flaps deflected from $0°$ to $100°$, two directions of propeller rotation, and spanwise variation of propeller thrust.

Test results show that lift coefficient increased and drag coefficient decreased as the wing tips were extended outboard. Maximum lift coefficient appeared to be limited by flow separation between the nacelles on all configurations, even though the wing tip of the high aspect ratio configuration was not protected by the propeller slipstream. Leading-edge slats controlled the progression of flow separation and extended the angle of attack for maximum lift approximately $10°$ (e.g., for a thrust coefficient of 2.5, the angle of attack for maximum lift for the $80°$ flaps on the short wing was extended from $16°$ to approximately $25°$).

For each wing span tested descent capability could be improved by span-wise variation of propeller thrust. However, the spanwise variation of propeller thrust was most effective on the short span wing.

INTRODUCTION

Reference 1 indicated there was a lack of systematic experimental results to aid in the design of advanced propeller driven STOL aircraft. Ames Research Center therefore studied a large-scale deflected slipstream configuration in the 40- by 80-foot wind tunnel. The model employed in the study is typical of a conventional propeller-driven transport airplane capable of operating in and out of 1000 to 2000 foot runways.

The objectives of this investigation were to: (1) determine the basic longitudinal aerodynamic characteristics of a model whose wing was partially or fully immersed in the propeller slipstream, (2) determine the effect of propeller rotation on the stall progression across the upper surface of the

wing, and (3) determine the effect of the spanwise variation of propeller thrust across the wing span on the lift and drag characteristics of the model.

NOTATION

b wing span, ft

c wing chord parallel to fuselage center line, ft

$\bar{c}$ mean aerodynamic chord, $\dfrac{2}{S} \displaystyle\int_0^{b/2} c^2 \, dy$, ft

C_D drag coefficient including thrust, $\dfrac{\text{measured drag}}{qS}$

C_L lift coefficient including thrust, $\dfrac{\text{measured lift}}{qS}$

C_m pitching-moment coefficient, $\dfrac{\text{pitching moment}}{qS\bar{c}}$

C_n normal-force coefficient

D propeller diameter, ft

J propeller advance ratio, $\dfrac{V}{nD}$

L lift including thrust, lb

n propeller rotational velocity, rps

q free-stream dynamic pressure, lb/sq ft

R Reynolds number, $\dfrac{\rho V \bar{c}}{\mu}$

r propeller blade radius, ft

S wing area, sq ft

T total thrust of all four propellers, lb

T'_c thrust coefficient, $\dfrac{T}{qS}$

V free-stream tunnel velocity, fps

X chordwise dimension from leading edge

Y vertical dimension perpendicular to chord

y lateral distance from airplane center line

α wing angle of attack, deg

β propeller blade angle, deg

β_I, β_O propeller blade angle at $3/4\ r$ for inboard and outboard propellers, respectively, deg

γ descent angle, deg

δ_f total aft flap deflection relative to local wing chord, deg

$\delta_f \frac{xx}{xx}$ differential spanwise flap deflection. Numerator is for flap inboard of midpoint between nacelles; denominator is for flap outboard

$$\left(e.g., \quad \delta_f \frac{100}{60} = \frac{100^\circ\ \text{inboard}}{60^\circ\ \text{outboard}} \right)$$

μ coefficient of viscosity, slugs/ft-sec

ρ mass density of air, slugs/ft^3

MODEL AND APPARATUS

Figures 1(a) and (b) are photographs of the model installed in the 40- by 80-foot test section. The model was tested, as shown, without a horizontal tail. Figure 2(a) is a three-view drawing of the model.

The airfoil section of the wing was an NACA 63_2-416 with the reflex on the aft portion of the lower surface faired out. The short wing span was 43.34 feet (fig. 2(a)) with an aspect ratio of 5.71. Short wing tip extensions changed the span to 47.94 feet, and longer tips extended the span to 56 feet with an aspect ratio of 8.06. Additional information about the wing and tail geometry is given in table I.

A cross section of the wing leading-edge slat and trailing-edge triple-slotted flap is shown in figure 2(b). The trailing-edge flap could be deflected 100° with respect to the wing chord line. For flap deflections of 80° or less, the foreflap was set at half the total deflection of the aft flap. For a flap deflection of 100°, the foreflap was deflected 40°. Coordinates for the wing leading-edge slat, trailing-edge foreflap, fixed vane, and aft flap are listed in table II.

The geometric characteristics of the three-bladed model propellers are presented in figure 3. The solid aluminum propellers were 9.3 feet in diameter and had an activity factor of 121 per blade. Each propeller was shaft mounted on a gearbox and driven by an electric motor. The four motors were operated in parallel from a variable frequency power supply.

TEST AND PROCEDURE

Tests were made at free-stream velocities from 31 to 49 knots ($q = 3.1$ to 8 psf, corresponding to a Reynolds number range of 2.4 to 4.1 million). During each run the angle of attack of the model was varied while the tunnel dynamic pressure, propeller speed, and propeller blade angle were held fixed.

The propeller thrust (fig. 4) was calibrated from wind-tunnel tests with the model at the angle of attack for zero lift with the flaps retracted. Propeller thrust was defined as the sum of the measured thrust of the model with the propellers operating and the measured drag of the model with propellers removed. For runs with all propellers set for equal thrust, the inboard and outboard propellers were set at a blade angle of $16°$ at the three-quarter radius station. To obtain the spanwise variation of propeller thrust the inboard propeller blade angle was left at $16°$ while the outboard propeller blade angle was set at $0°$. With this blade setting, and inboard thrust assumed to be independent of outboard thrust, the two inboard propellers produced a high positive value of thrust while the two outboard propellers gave a slightly negative value.

Aerodynamic coefficients were based on the flaps-retracted reference wing area for each of the three wing spans evaluated. Pitching-moment coefficients were computed about a moment center at $0.25 \bar{c}$.

CORRECTIONS

Cook and Hickey (ref. 1, p. 447) suggested applying standard wind-tunnel wall corrections for this size STOL model. The following corrections were made to account for the wind-tunnel wall interference effects:

Short-span wing

$$\alpha = \alpha_u + 0.652 \, C_{L_u}$$

$$C_D = C_{D_u} + 0.01138 \, C_{L_u}^2$$

Medium-span wing

$$\alpha = \alpha_u + 0.674 \, C_{L_u}$$

$$C_D = C_{D_u} + 0.01176 \, C_{L_u}^2$$

Long-span wing

$$\alpha = \alpha_u + 0.706 \, C_{L_u}$$

$$C_D = C_{D_u} + 0.01232 \, C_{L_u}^2$$

The subscript u stands for measured results uncorrected for wind-tunnel wall effects.

A drag tare correction ($\Delta C_D \approx 0.03$) was applied to account for the drag of the portions of the mounting struts exposed to the wind-tunnel air flow.

RESULTS

The main results of this investigation are summarized in figures 5 through 10. These figures are briefly discussed in the next section. In the interest of completeness, the basic data are presented (without discussion) in figures 11 through 13. Figure 11 presents the data for the short-span wing; figure 12 presents the data for the medium-span wing; and figure 13 presents the data for the long-span wing. Table III is an index to these basic data figures.

DISCUSSION

Figures 5(a)[1] and (b) present the lift and drag coefficients for the three wing spans with trailing-edge flaps deflected 80° for two thrust coefficients. Figure 5(c) presents the effect of the leading-edge slats in extending the lift curves, with only the top portion of the curves shown for clarity. These data show that, as the wing tips were extended, lift coefficient increased and the drag coefficient decreased. Lift coefficient increased with wing span even though the portion of the wing outside the slipstream was not as highly loaded as that inside the slipstream. Some insight into this result is obtained from the pressure distribution data (ref. 2). Figures 6(a) and (b) present the span loading (normal-force coefficient versus spanwise position) of a short-span wing compared with the longer span wing and show that as the tip is extended beyond the slipstream, there is an additional increment of "lift carryover" from the tip inboard.

The angle of attack for maximum lift was limited by flow separation between the nacelles. The onset of flow separation occurred just forward of the foreflap (0.7c) on the upper surface of the wing. With the first direction of propeller rotation (i.e., ⌒• ⌒• ⌒• ⌒•), separation began at low positive angles of attack and progressed rapidly to the leading edge of the wing. With the second direction of propeller rotation (i.e., ⌒• ⌒• ⌒• ⌒•) tuft observations indicated that separation was delayed, but this effect was not reflected in the force data. The leading-edge slats prevented this forward progression of flow separation, and the angle of attack for maximum lift was extended approximately 10°.

---

[1]On figure 5(a) the data for the long span wing were interpolated from measurements obtained at T'_c = 0, 2.0, and 4.0.

Incremental flap lift coefficient and drag coefficient as a function of flap deflection are presented in figures 7 and 8 for the medium-span wing for three thrust coefficients, with the leading-edge slats retracted, and for an angle of attack of 0°. Figure 7 shows that the flap effectiveness approached theoretical values for $T'_c = 0$ (ref. 3) up to flap deflections of 60°.

Figure 9 presents the variation of drag with maximum lift coefficient for the three wing spans with leading-edge slats extended, 80° flap deflection, three values of thrust coefficient, and with and without spanwise variation of propeller thrust. In terms of descent performance, the 80° flaps appeared to be optimum for all configurations tested at equal approach speeds. The results presented in figure 9 show that spanwise variation of propeller thrust greatly increased descent angle (e.g., for a constant lift coefficient of 7 the descent angle was approximately doubled with $T'_{c_{av}} = 1.5$ compared to $T'_c = 2.5$). For a given C_L, descent angle decreased as the wing span was extended. Also, as the wing span was extended, spanwise variation of propeller thrust became less effective as a means of increasing descent capabilities.

Since the model with the medium span wing resembles the aircraft in the flight report of reference 4, a comparison of $C_{L_{max}}$ for the model and for the flight aircraft is presented in figure 10. The comparison is made for a landing configuration (δ_f 100/60 model; δ_f 98/65 flight) with and without leading-edge slats installed on the model. The wing leading edge on the flight aircraft had a drooped nose (4.5 percent extended chord) outboard of the inboard nacelle, whereas the model had full span 0.2c slats as shown in figure 2(b). The correlation appears to be reasonable since the flight data fall between the wind-tunnel data for the slats retracted and slats extended configurations.

CONCLUDING REMARKS

As the wing tips were extended beyond the immersed portion of the wing, lift coefficient increased and drag coefficient decreased. For a given landing configuration, the descent angle decreased as the wing tip was extended. Spanwise variation of propeller thrust was effective in increasing descent capability, but was most effective when used on the short span wing that was fully immersed in the propeller slipstream. Maximum lift coefficient appeared to be limited by flow separation between the nacelles - not by flow separation over the unimmersed wing tips.

Leading-edge slats were effective in controlling flow separation and, for each wing span tested, extended the angle of attack for maximum lift approximately 10°. In addition, the use of leading-edge slats allowed an increase in the angle of descent and rate of sink for a constant approach speed.

Ames Research Center
    National Aeronautics and Space Administration
        Moffett Field, Calif., 94035, Nov. 16, 1967
            721-01-00-16-00-21

REFERENCES

1. Conference on V/STOL and STOL Aircraft, April, 1966. NASA SP-116, 1966.

2. Page, V. Robert; and Soderman, Paul T.: Wing Surface Pressure Data From Large-Scale Wind Tunnel Tests of a Propeller-Driven STOL Model. NASA TM X-1527, 1968.

3. DeYoung, John: Theoretical Symmetric Span Loading Due to Flap Deflection for Wings of Arbitrary Plan Form at Subsonic Speeds. NACA Rep. 1071, 1952 (Supersedes NACA TN 2278).

4. Quigley, Hervey C.; Innis, Robert C.; and Holzhauser, Curt A.: A Flight Investigation of the Performance, Handling Qualities, and Operational Characteristics of a Deflected Slipstream STOL Transport Airplane Having Four Interconnected Propellers. NASA TN D-2231, 1964.

TABLE I. - MODEL GEOMETRY

Dimension	Wing span			Vertical tail
	Short	Medium	Long	
Area, sq ft	329	352.8	389.3	86.9
Span, ft	43.34	47.94	56	11.22
Mean aerodynamic chord, ft	7.80	7.62	7.30	8.26
Aspect ratio	5.71	6.52	8.06	1.45
Taper ratio	0.554	0.507	0.424	0.389
Twist, deg	0	0	0	0
Dihedral, deg	0	0	0	0
NACA airfoil section	63_2-416	63_2-416	63_2-416	63A013
Sweep of leading edge, deg	2.88	2.88	2.88	31.33
Sweep of trailing edge, deg	-8.57	-8.57	-8.57	0
Root chord, ft	9.77	9.77	9.77	11.17
Tip chord, ft	5.41	4.95	4.14	4.34

TABLE II.- COORDINATES OF LEADING-EDGE SLAT AND TRAILING-EDGE TRIPLE
SLOTTED FLAP, PERCENT CHORD

Leading-edge slat[1]			Trailing-edge foreflap[2]		
X	Y_U	Y_L	X	Y_U	Y_L
0	0.40	---	0	0	0
.25	1.50	---	.15	.9	-1.25
.50	1.98	---	.3	1.32	-1.62
.75	2.34	---	.5	1.73	-2.0
1.00	2.63	---	.75	2.15	-2.35
1.50	3.12	---	1.0	2.5	-2.60
2.00	3.50	---	2	3.44	-3.14
2.50	3.78	---	3	4.13	-3.32
3	4.02	---	4	4.62	-3.28
4	4.37	0.52	5	4.97	-3.18
5	4.58	1.47	6	5.22	-3.09
6	4.66	2.08	7	5.38	-3.00
7	4.65	2.49	8	5.49	-2.90
8	4.57	2.74	9	5.53	-2.81
10	4.17	2.88	10	5.52	-2.72
12	3.58	2.69	12.6	5.33	-2.48
14	2.84	2.25	12.76	5.30	0
16	1.98	1.62	15	4.92	2.50
18	1.07	.80	17.5	4.42	3.53
20	.08	-.08	20	3.85	3.80

Trailing-edge vane[3]			Trailing-edge aft flap[4]		
0	0	0	0	0	0
.1	.44	-.36	.25	1.12	-.9
.2	.63	-.50	.5	1.58	-1.24
.3	.77	-.58	.75	1.92	-1.45
.4	.88	-.65	1	2.16	-1.62
.5	1.00	-.68	1.5	2.5	-1.78
.75	1.18	-.68	2	2.77	-1.83
1.0	1.33	-.6	2.5	2.95	-1.80
1.5	1.52	-.3	3	3.08	-1.76
2	1.62	.04	4	3.21	-1.66
2.5	1.62	.32	5	3.25	-1.57
3	1.57	.48	7.5	2.85	-1.33
3.5	1.46	.53	10	2.35	-1.08
4	1.28	.53	12.5	1.85	-.85
4.5	1.06	.47	15	1.33	-.62
5	.78	.36	17.5	.83	-.37
5.5	.45	.20	20	.32	-.15
6.0	.1	.03	21.4	.02	-.03
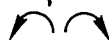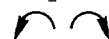
[1]Leading-edge radius = 1.9; slope of radius line through leading edge of
slat = 0.20
[2]Leading-edge radius = 3.0
[3]Leading-edge radius = 0.85
[4]Leading-edge radius = 1.8

TABLE III.- FIGURE INDEX TO BASIC DATA

Figure	Wing span	Flap deflection	Leading edge	Rotation
11(a)	Short	0	Clean	Propellers off
(b)		0		
(c)		20		
(d)		40		
(e)		60		
(f)		80		
(g)		80	Full span slats	
(h)		80	Slats outboard of inboard nacelle	
(i)		40/20	Clean	Differential propeller thrust
(j)		60/40		
(k)		100/60		
12(a)	Medium	0		Propellers off
(b)		0		
(c)		40		
(d)		40	Full span slats	
(e)		80	Clean	
(f)		80	Full span slats	
(g)		80	Full span slats	Differential propeller thrust
(h)		100	Clean	
(i)		100	Full span slats	
(j)		100/60	Clean	
(k)		100/60	Full span slats	
(l)		100/60	Full span slats	Differential propeller thrust
13(a)	Long	80	Clean	
(b)		80	Full span slats	
(c)		80	Clean	Differential propeller thrust
(d)		80	Full span slats	Differential propeller thrust
(e)		100/60	Full span slats	
(f)		100/60	Full span slats	Differential propeller thrust
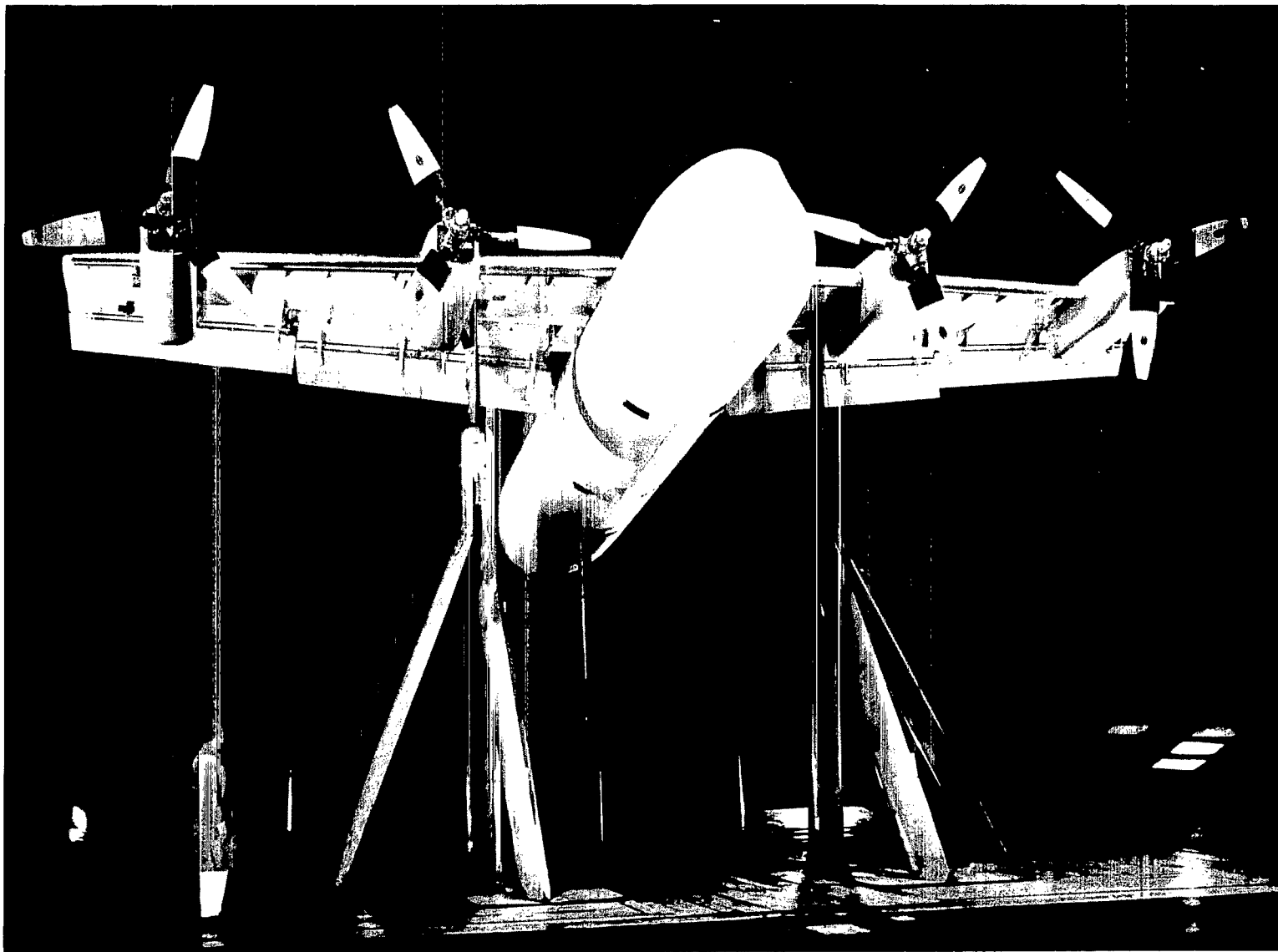
(a) Front view.

Figure 1.- Model in the Ames 40- by 80-Foot Wind Tunnel.
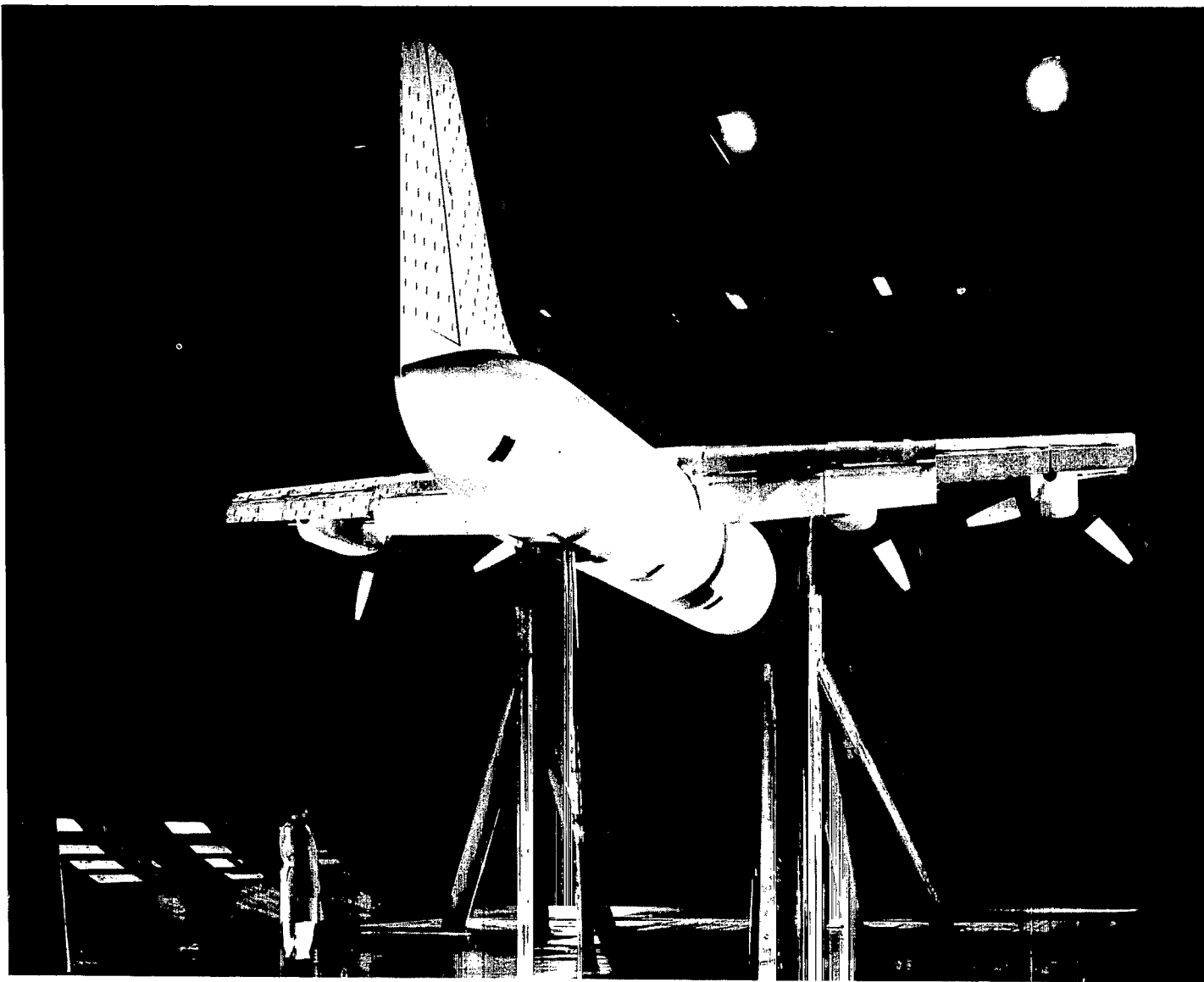
(b) Rear view.

A-37369

Figure 1.- Concluded.
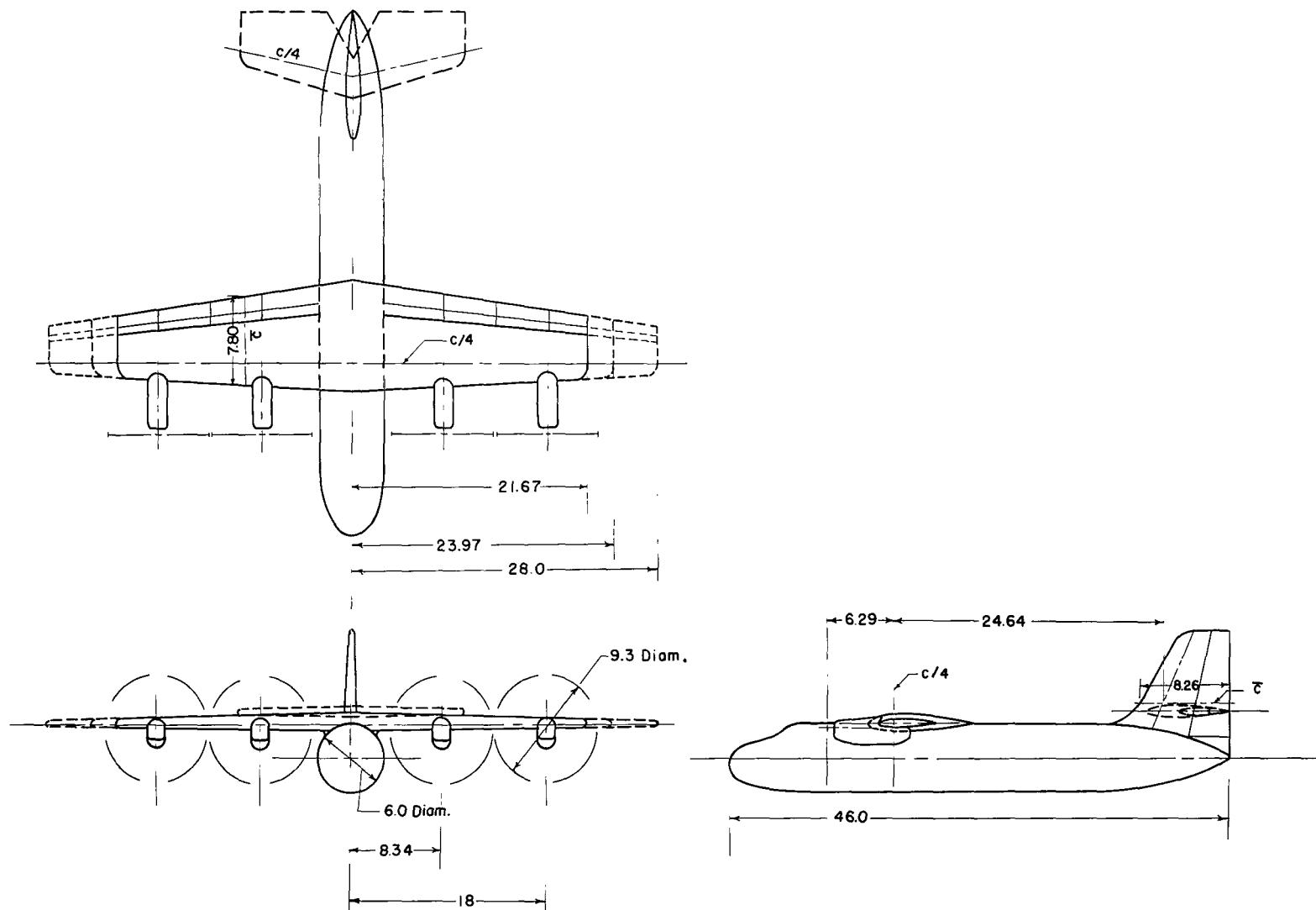
(a) Three views of model; dimensions in feet.

Figure 2.- Model geometry.

.01c

.02c

.2 c

45°

.2 c

Foreflap
hinge line
X = .692 c
Y = -.083c

Aft flap
hinge line
X = .815c
Y = -.0538c

$\delta_{foreflap}$

$\delta_{aft\ flap}$

.245c

$\delta_f = 100°$
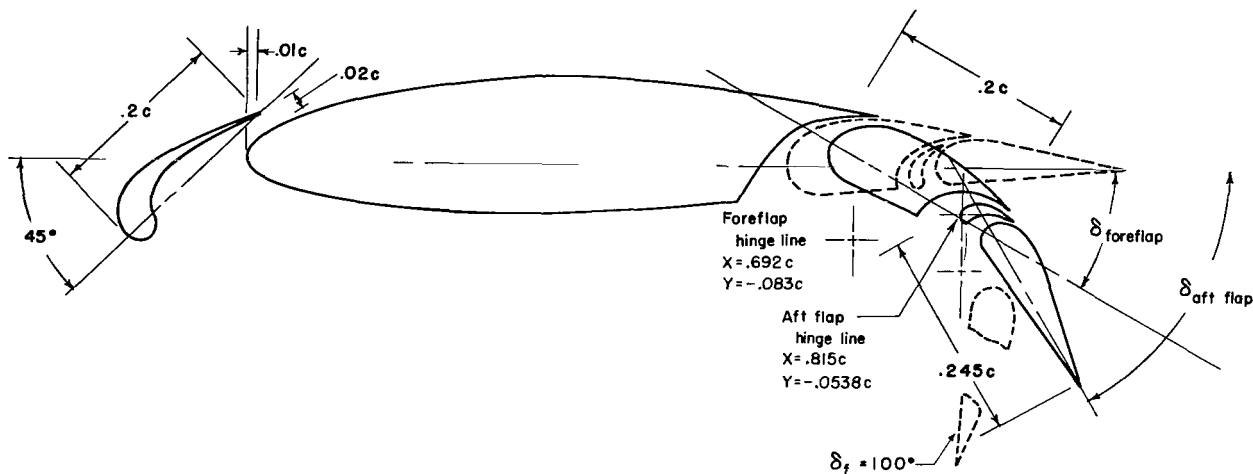
(b) Geometry of leading-edge slat and triple-slotted flap.

Figure 2.- Concluded.

Activity factor = 121/blade

Disk area = 67.9 ft^2/propeller

β

t/w

$\frac{t/w,\ Blade\ thickness}{Blade\ width}$

β, blade angle, deg

Fraction of blade radius
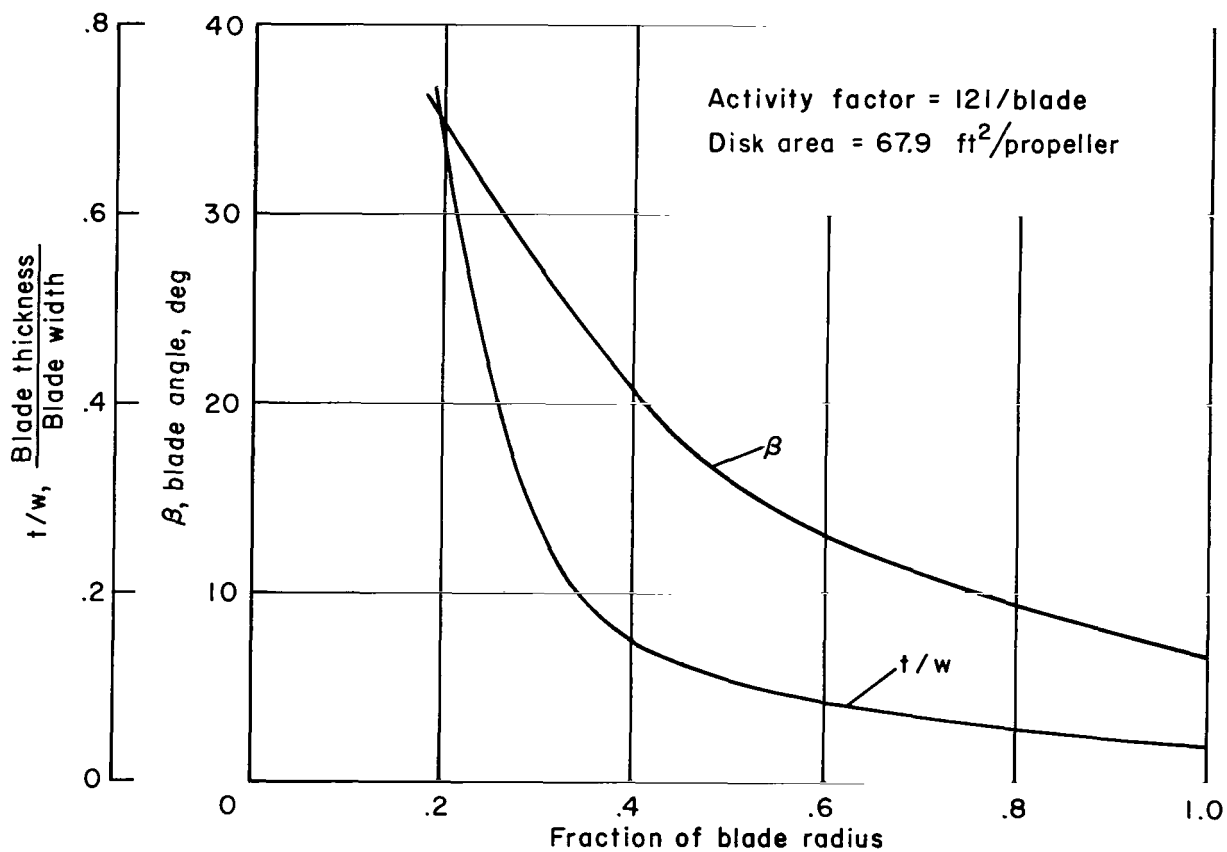
Figure 3.- Propeller blade characteristics.
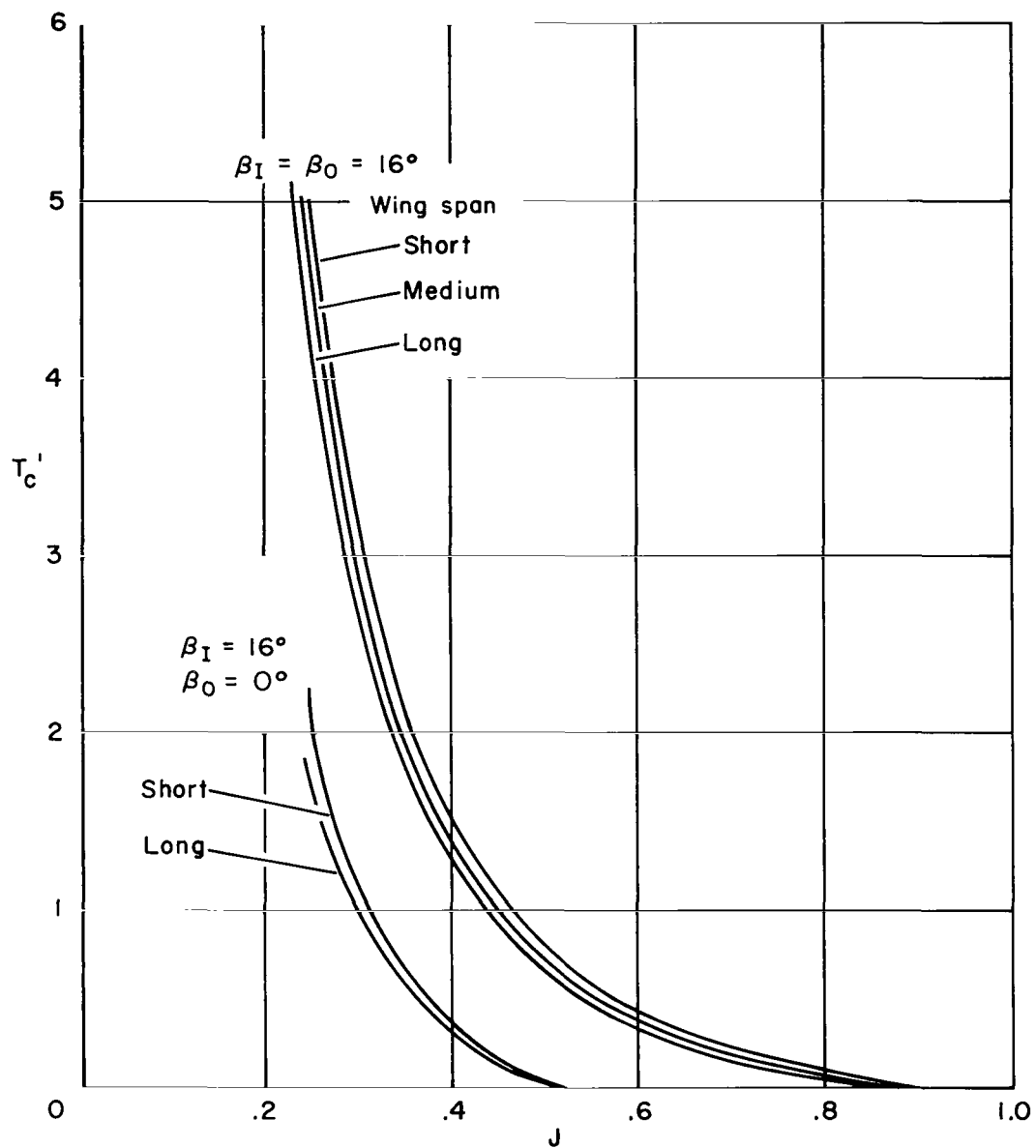
Figure 4.- Variation of propeller thrust coefficient with propeller advance ratio.
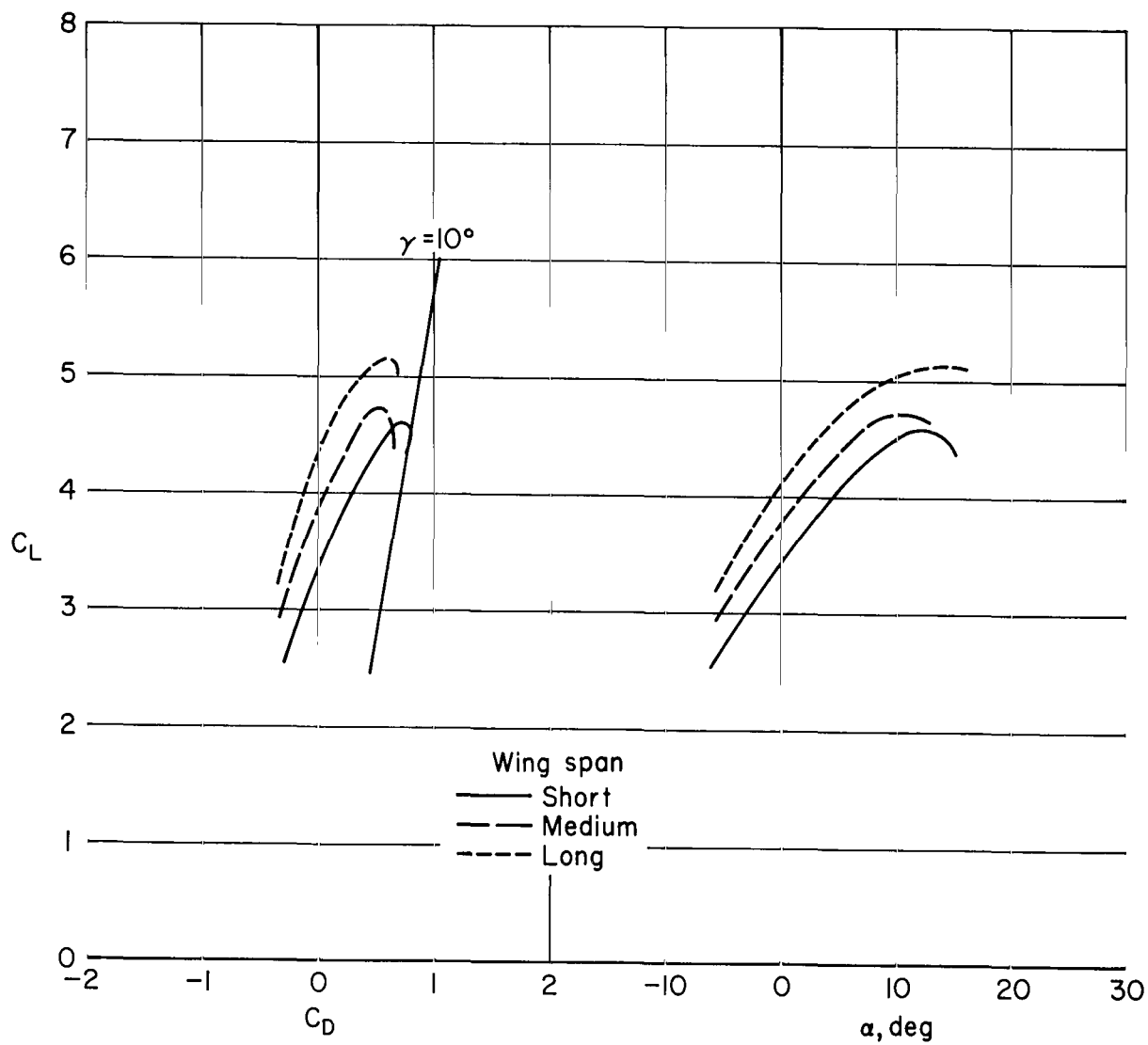
(a) $T_c' = 1.0$, clean leading edge.

Figure 5.- Variation of lift with drag and angle of attack for three wing spans, with 80° flap deflection.
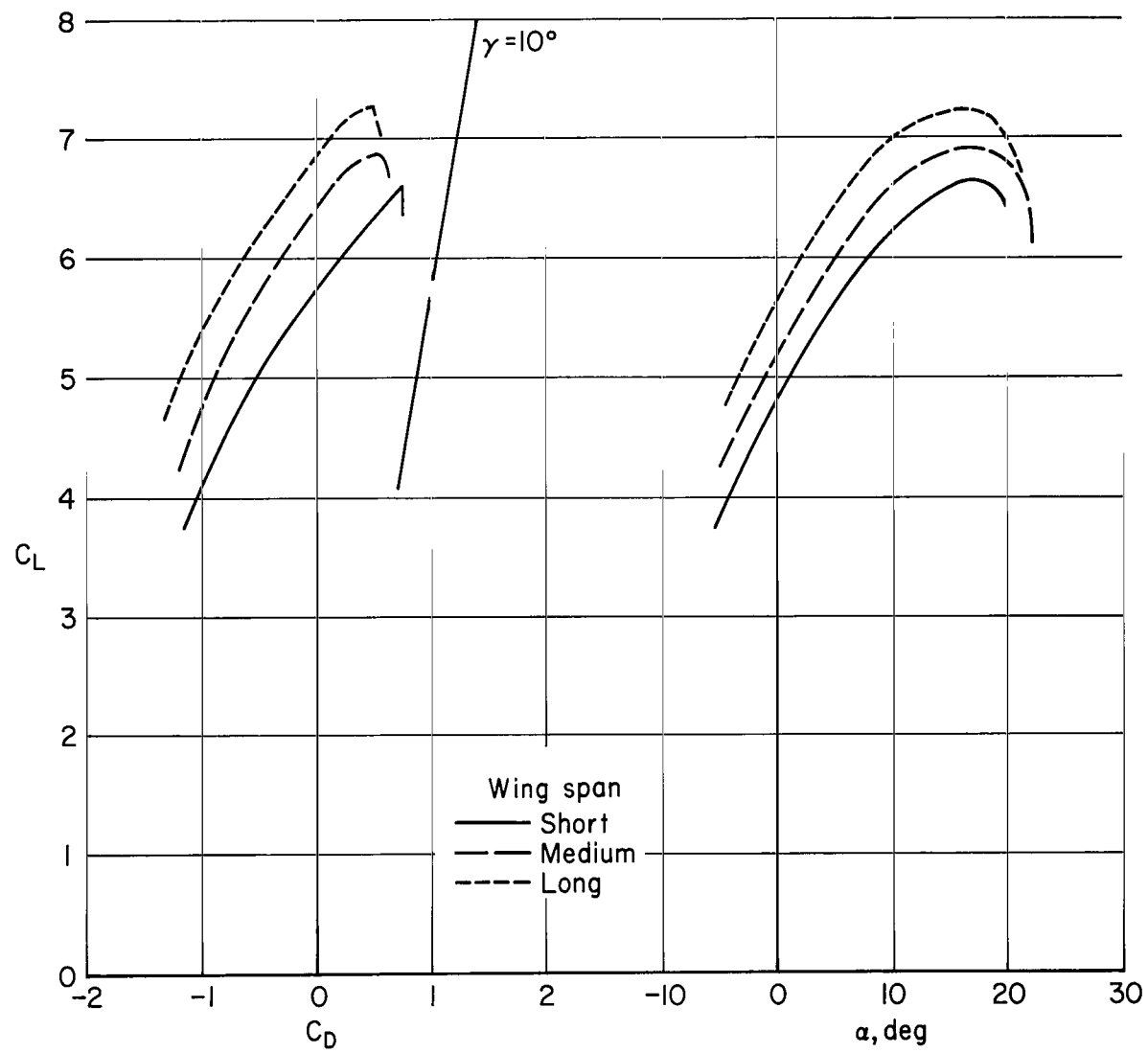
(b) $T_c' = 2.5$, clean leading edge.

Figure 5.- Continued.

(c) Effect of slats.
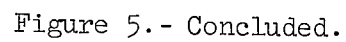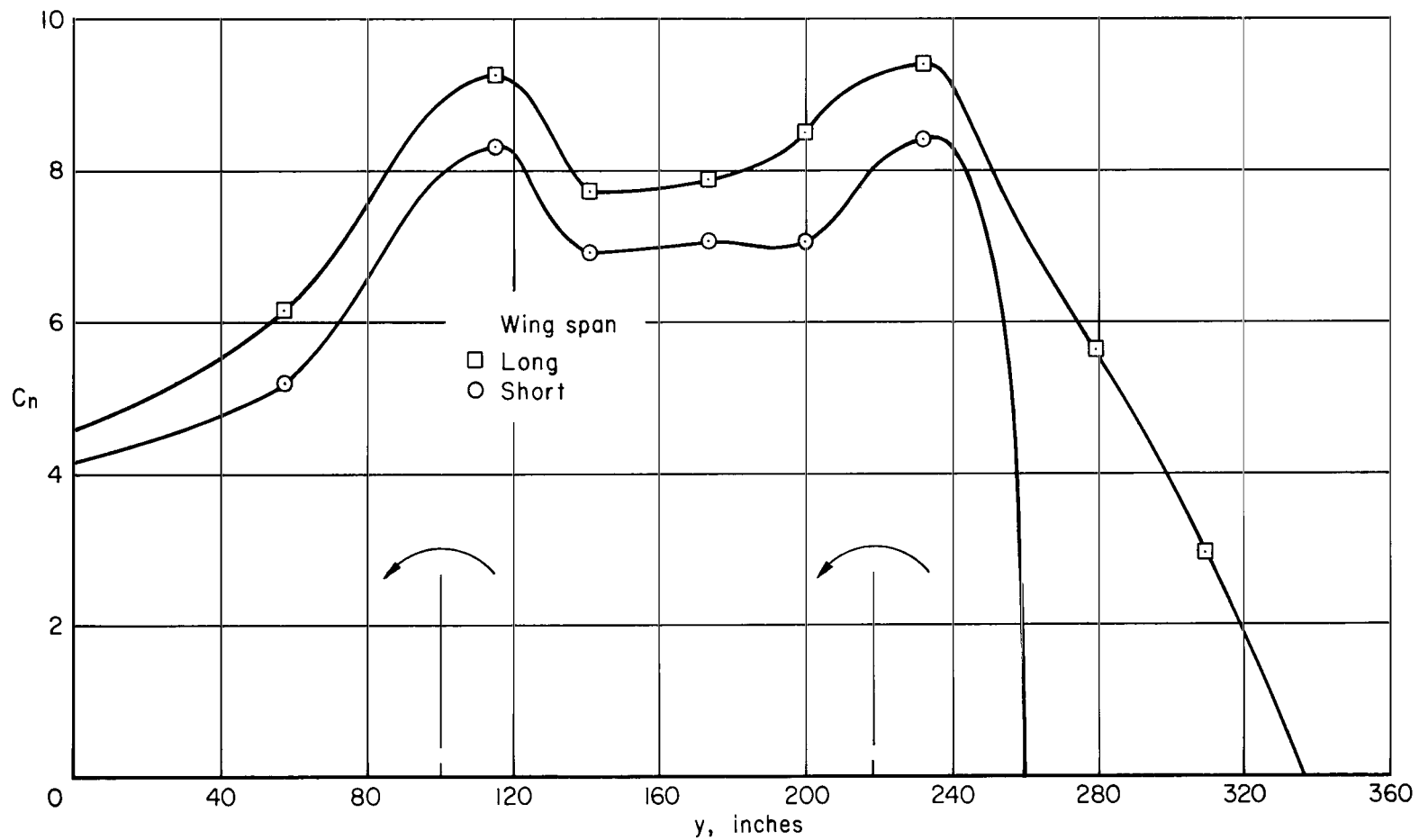
Figure 5.- Concluded.

(a) Clean leading edge.

Figure 6.- Variation of normal force with span position, 80° flap deflection, $T_c' = 2.5$, $\alpha = 0^\circ$.
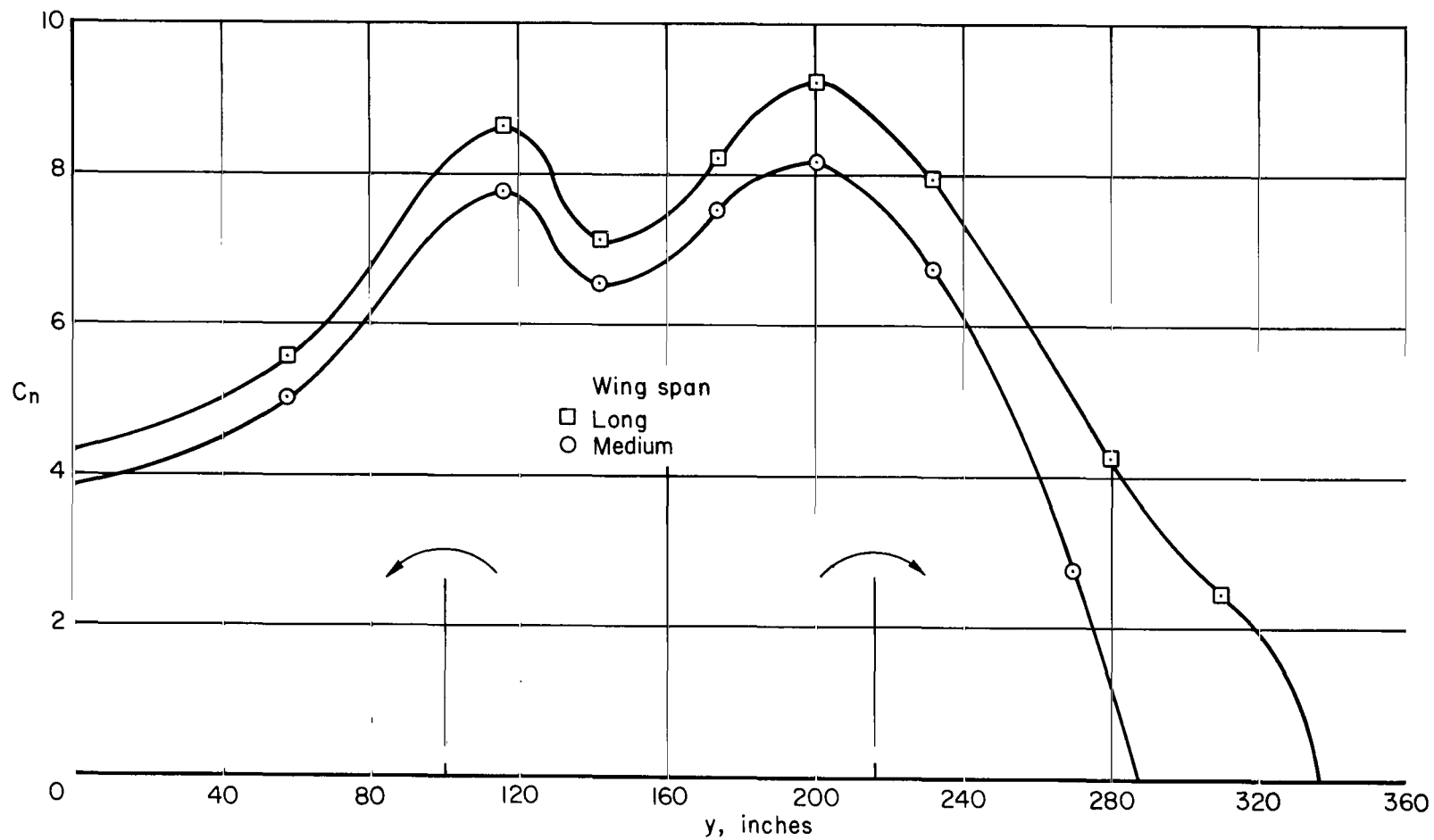
(b) With leading-edge slats.

Figure 6.- Concluded.
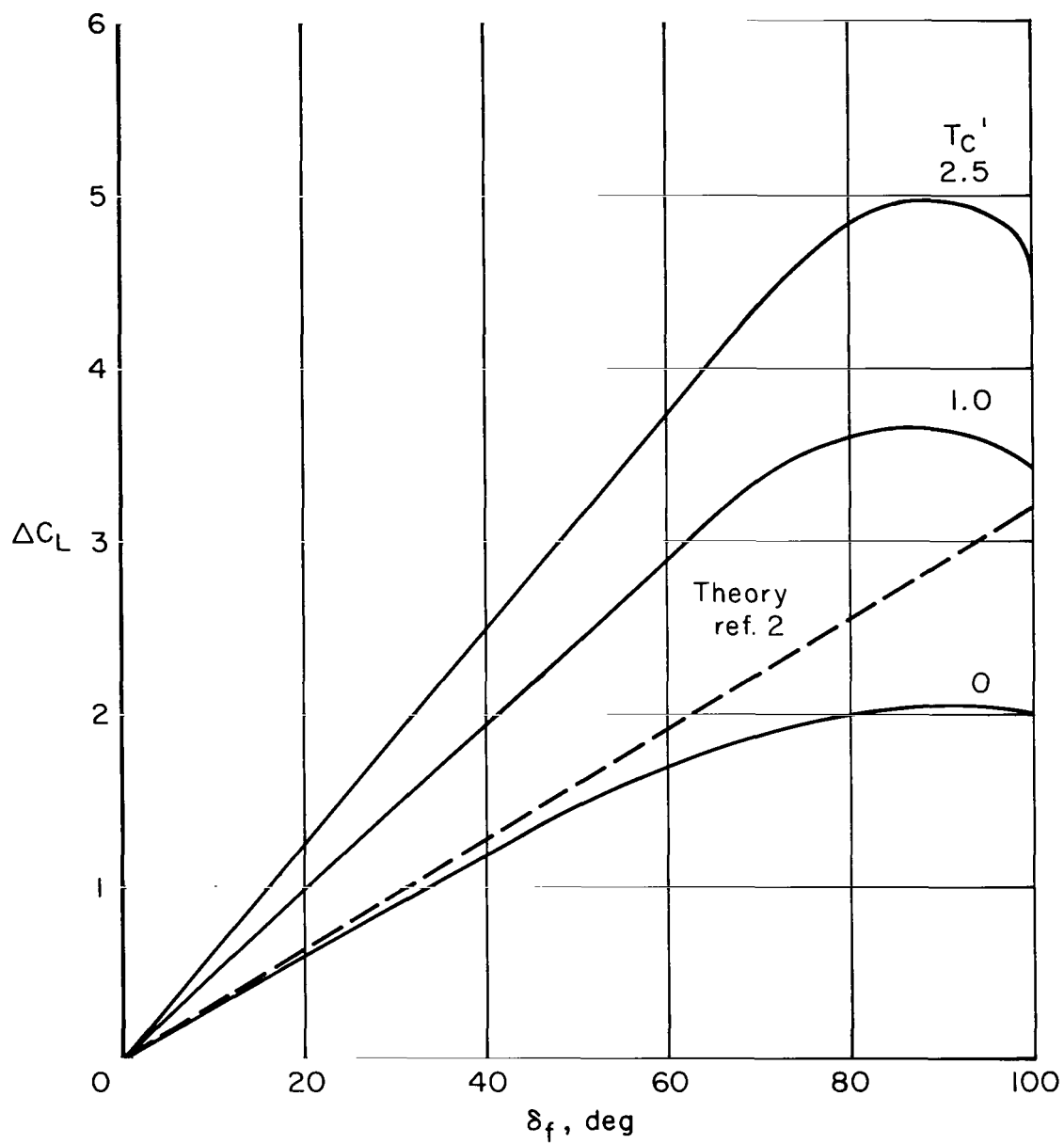
Figure 7.- Variation of flap lift increment with flap deflection for three thrust coefficients, clean leading edge, $\alpha = 0^{\circ}$, medium span wing.
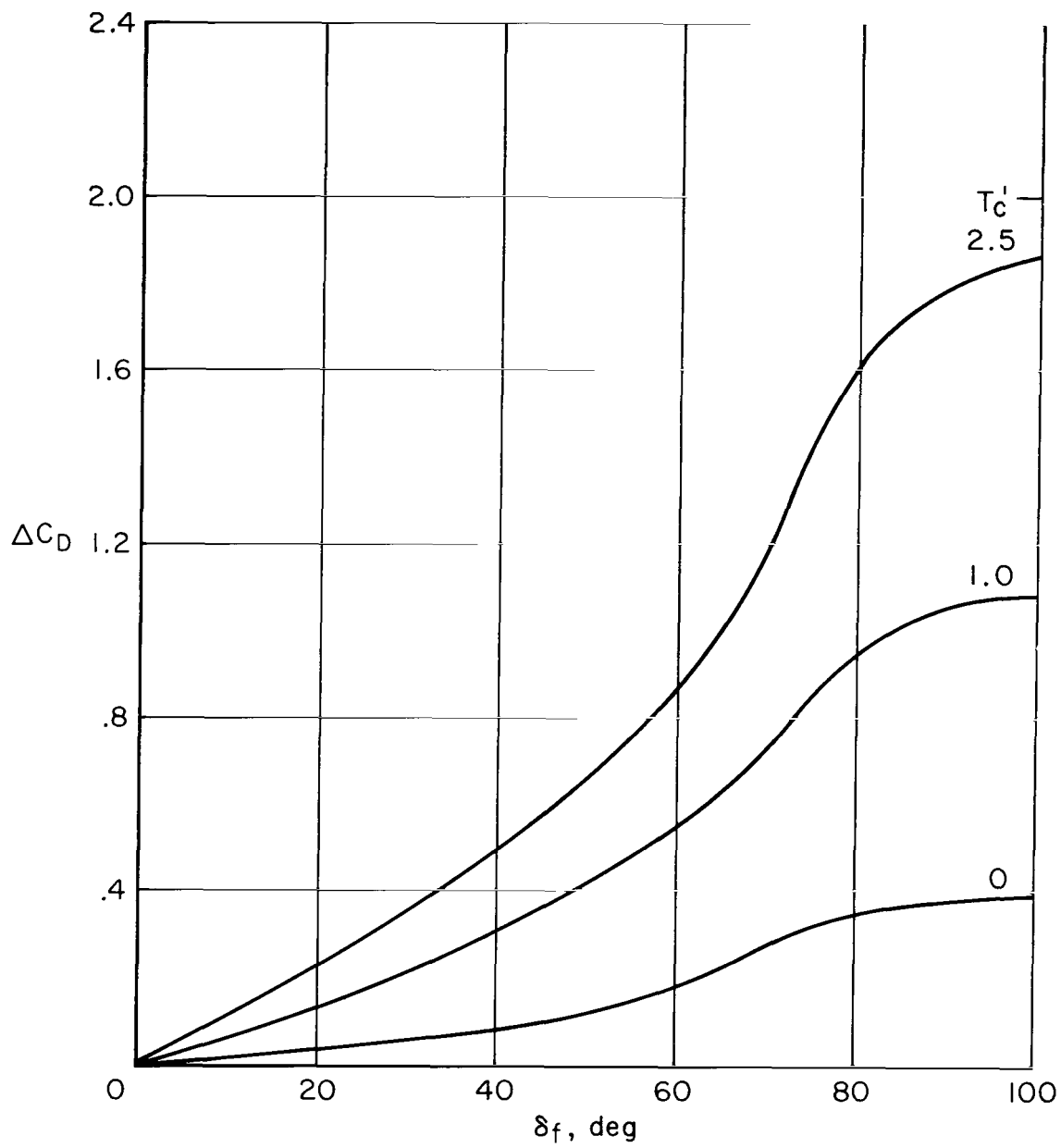
Figure 8.- Variation of flap drag increment with flap deflection, clean
leading edge, $\alpha = 0^{\circ}$, medium span wing.
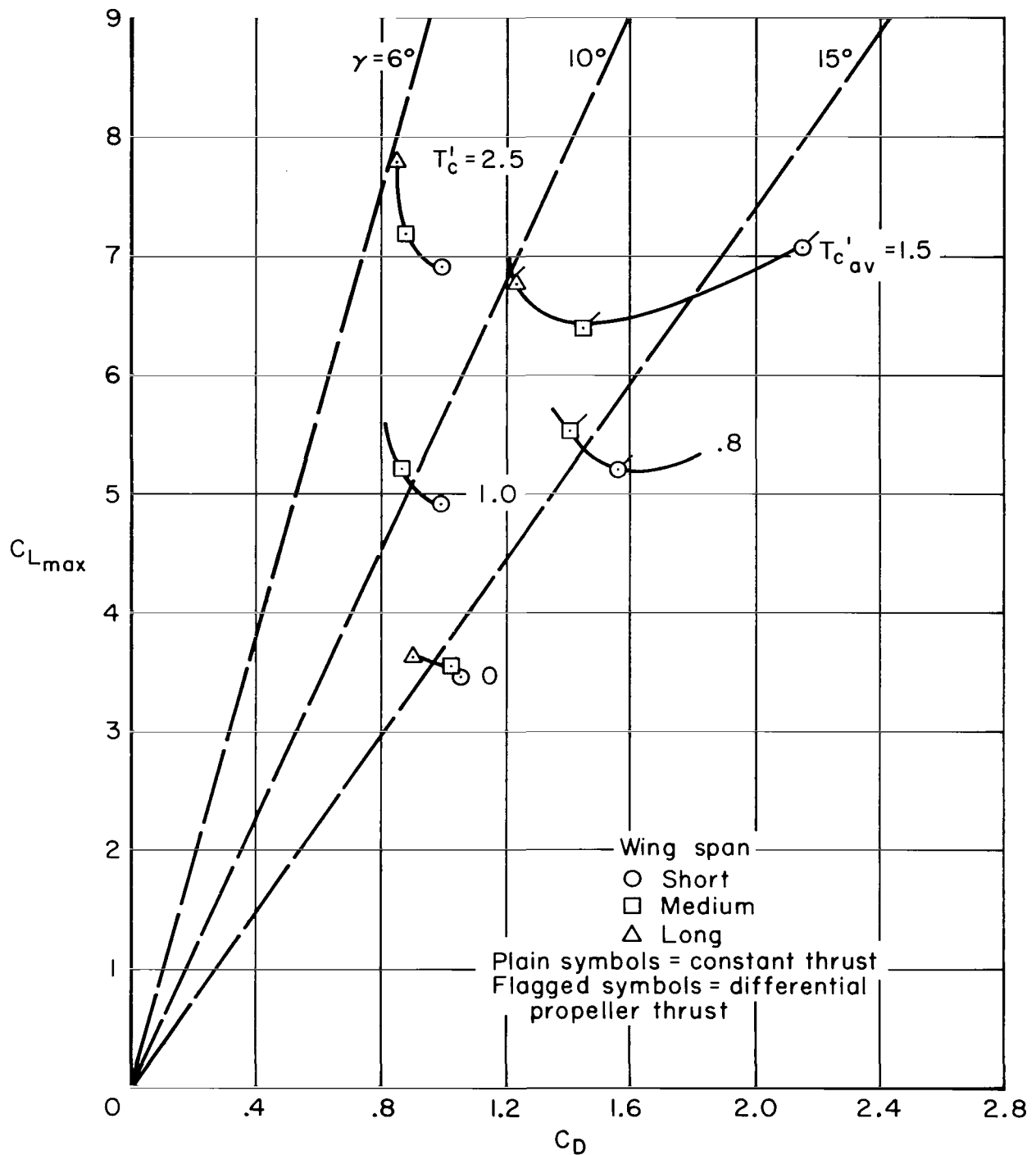
Figure 9.- Variation of drag at maximum lift for three wing spans, 80° flap
deflection, with leading-edge slats extended, with and without spanwise
variation of propeller thrust.
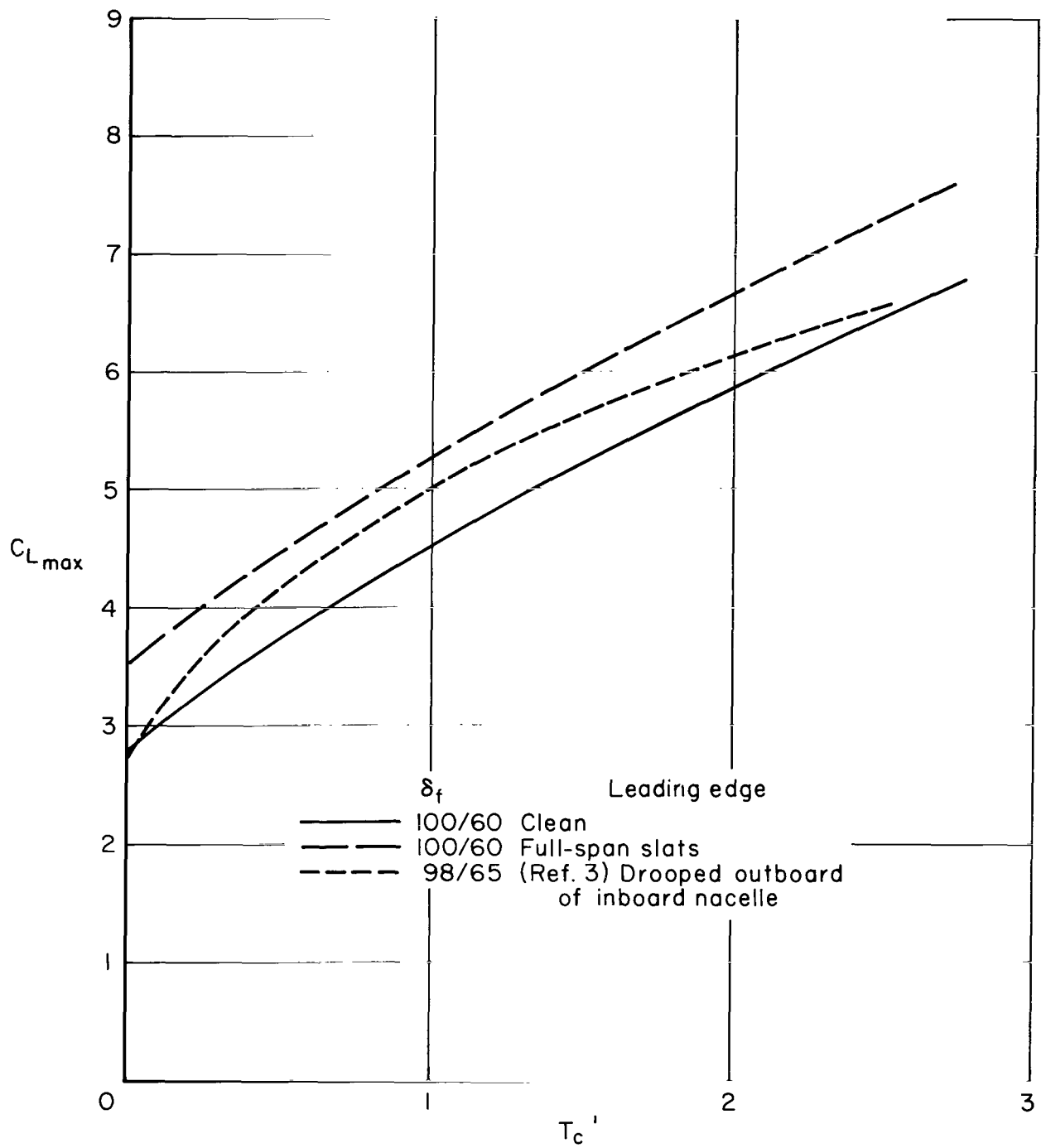
Figure 10.- Variation of $C_{L_{max}}$ with thrust coefficient for the model with the medium span wing as compared with the aircraft of reference 3.
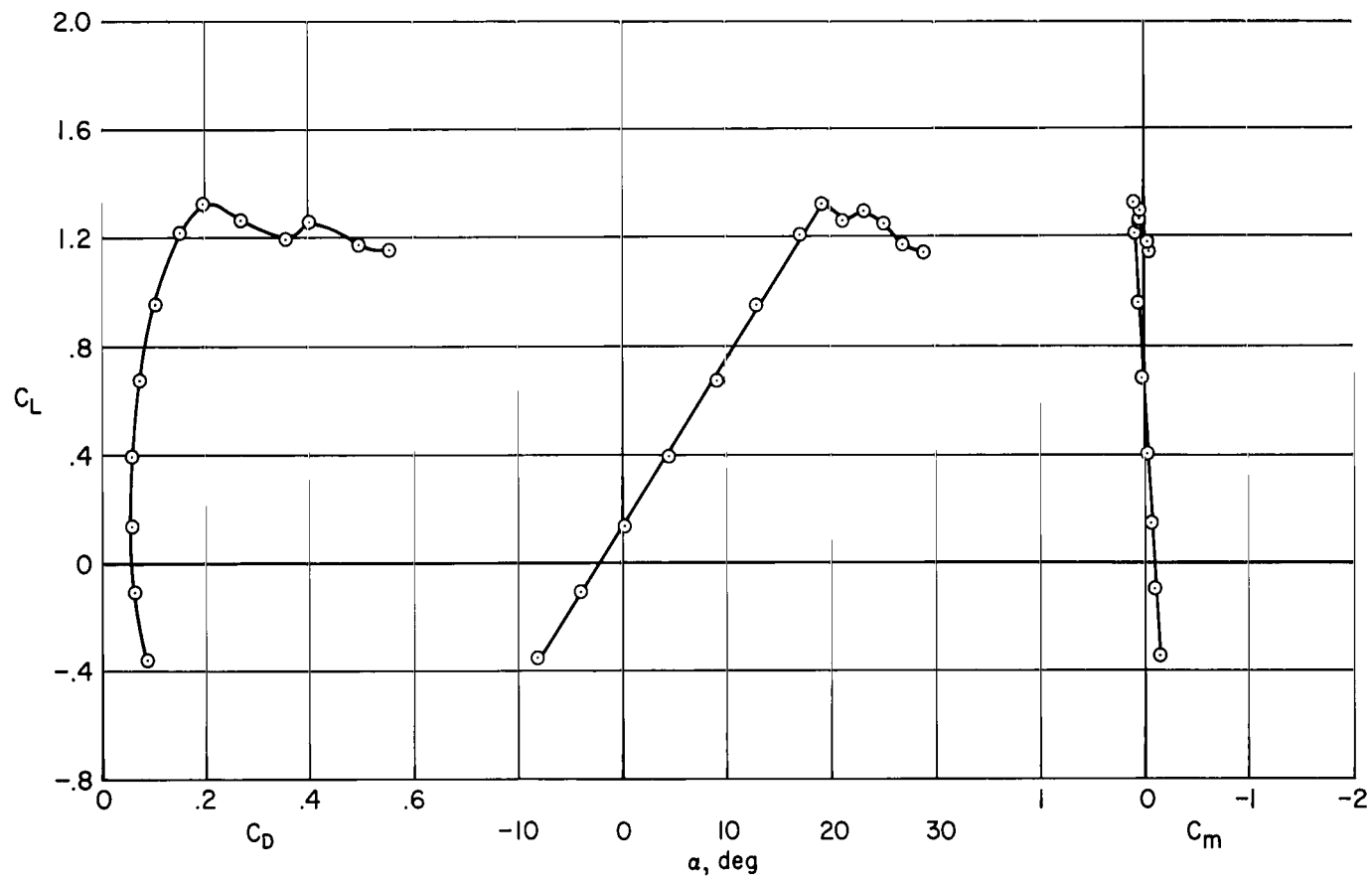
(a) $\delta_f = 0°$, propellers off, clean leading edge.

Figure 11.- Longitudinal characteristics of the model with the short-span wing; tail off.
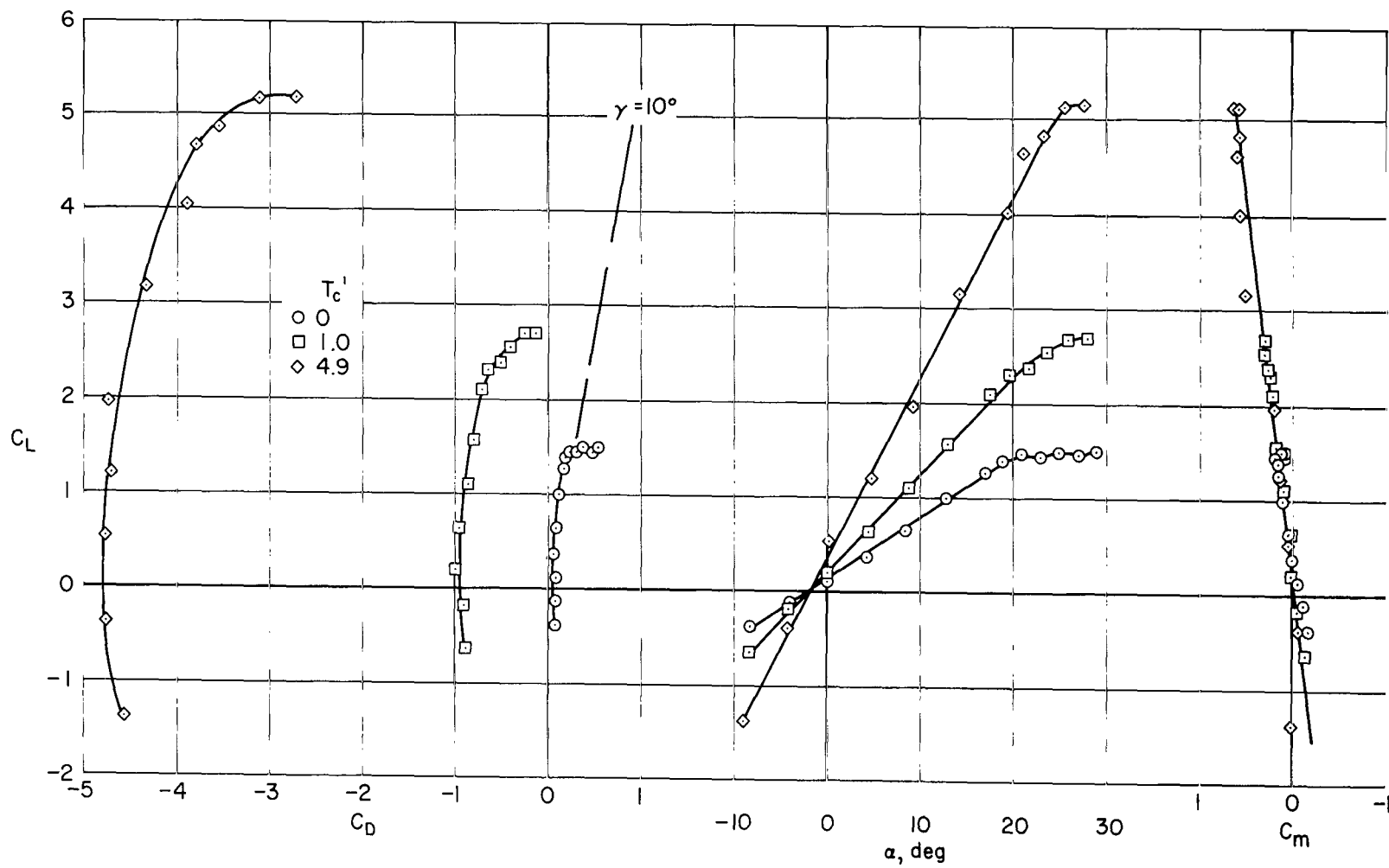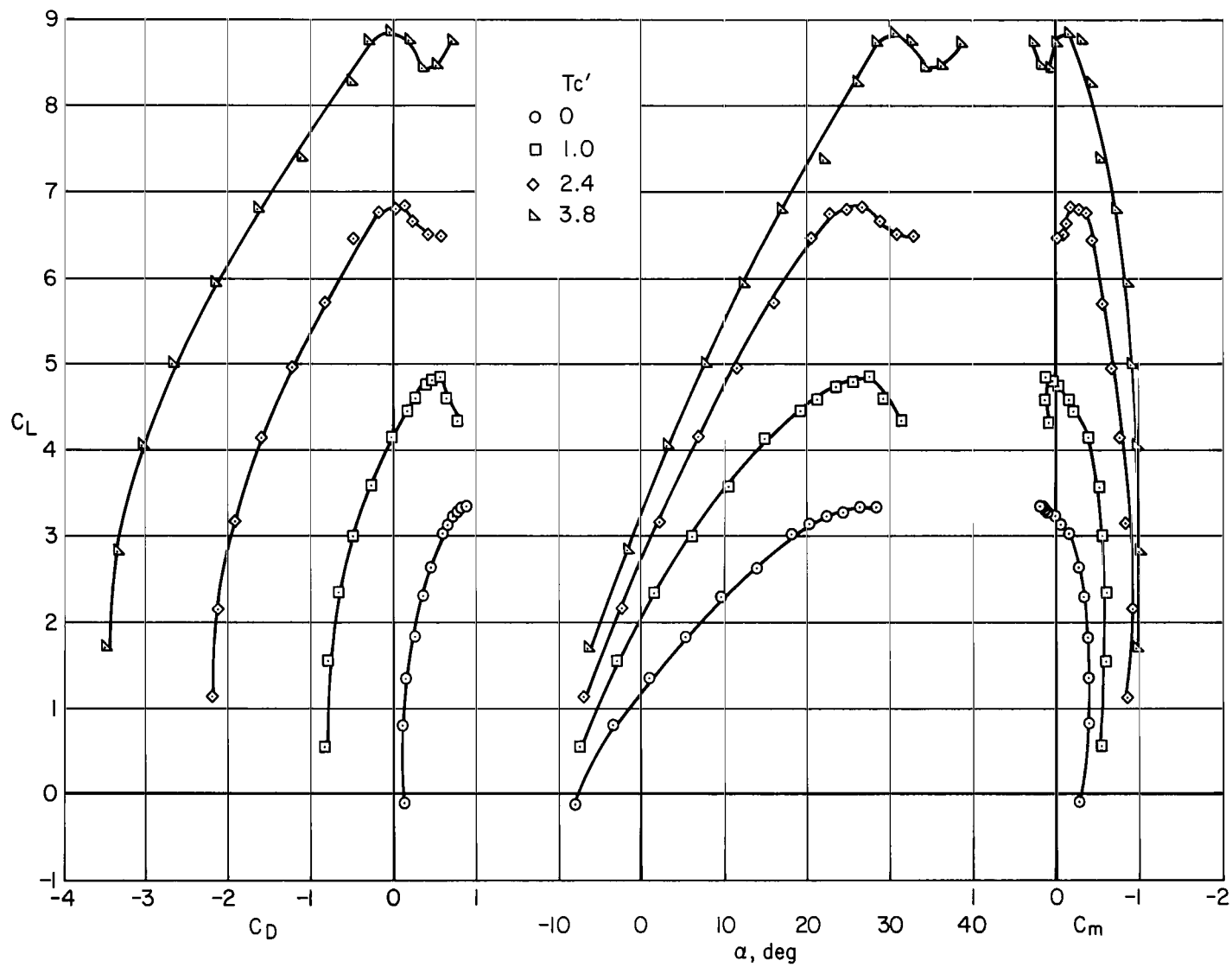
(b) $\delta_f = 0°$, clean leading edge.

Figure 11.- Continued.
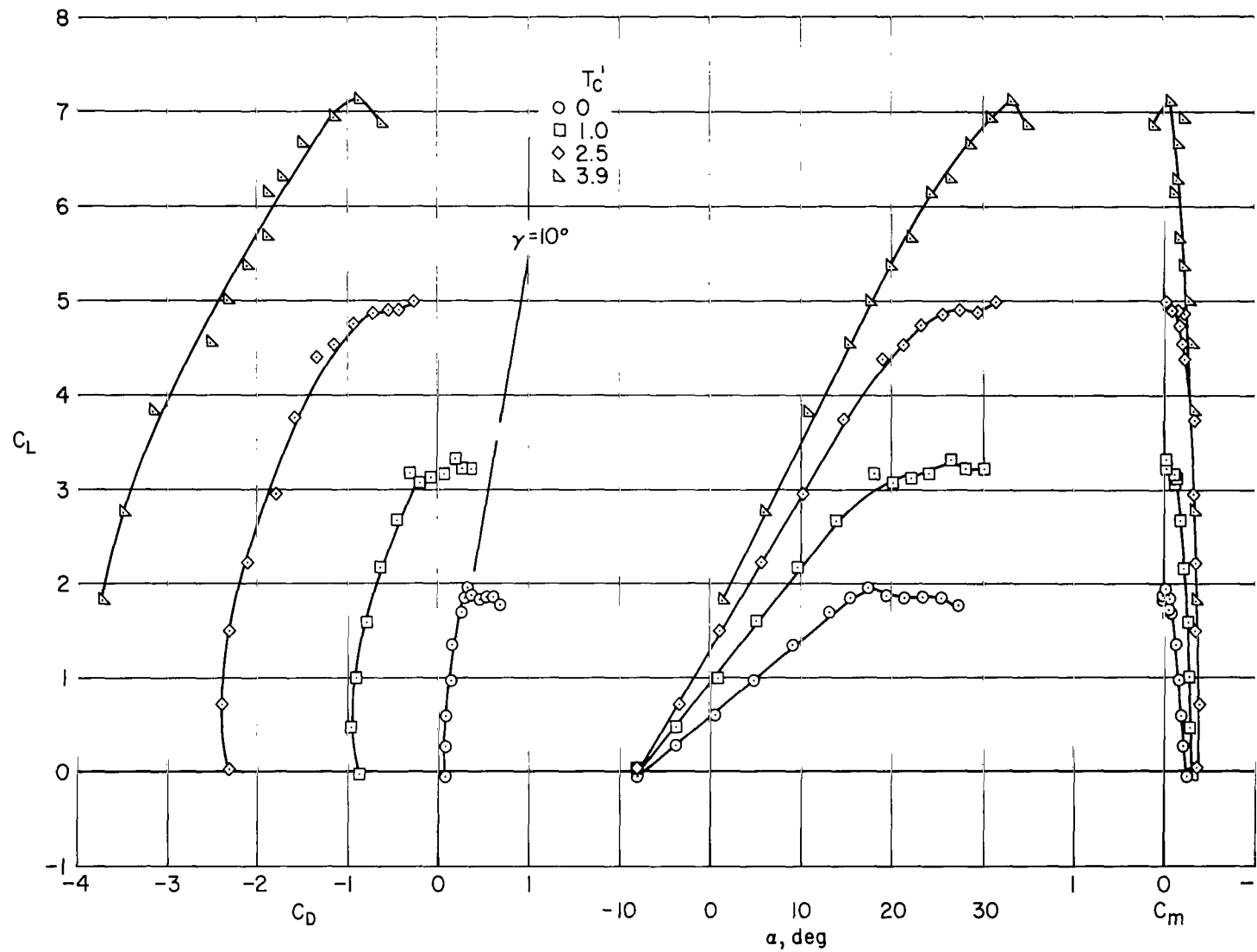
(c) $\delta_f = 20°$, clean leading edge.

Figure 11.- Continued.
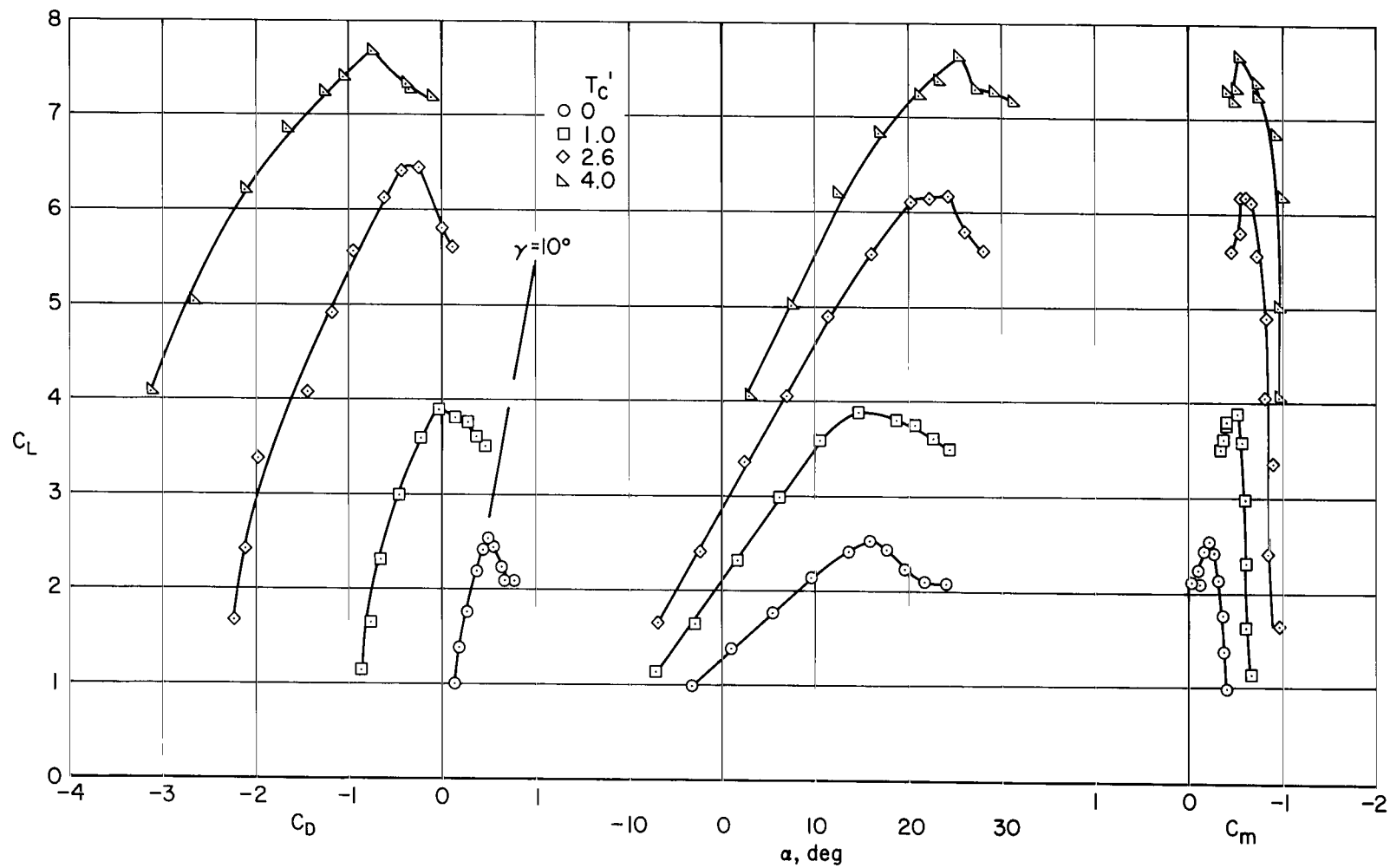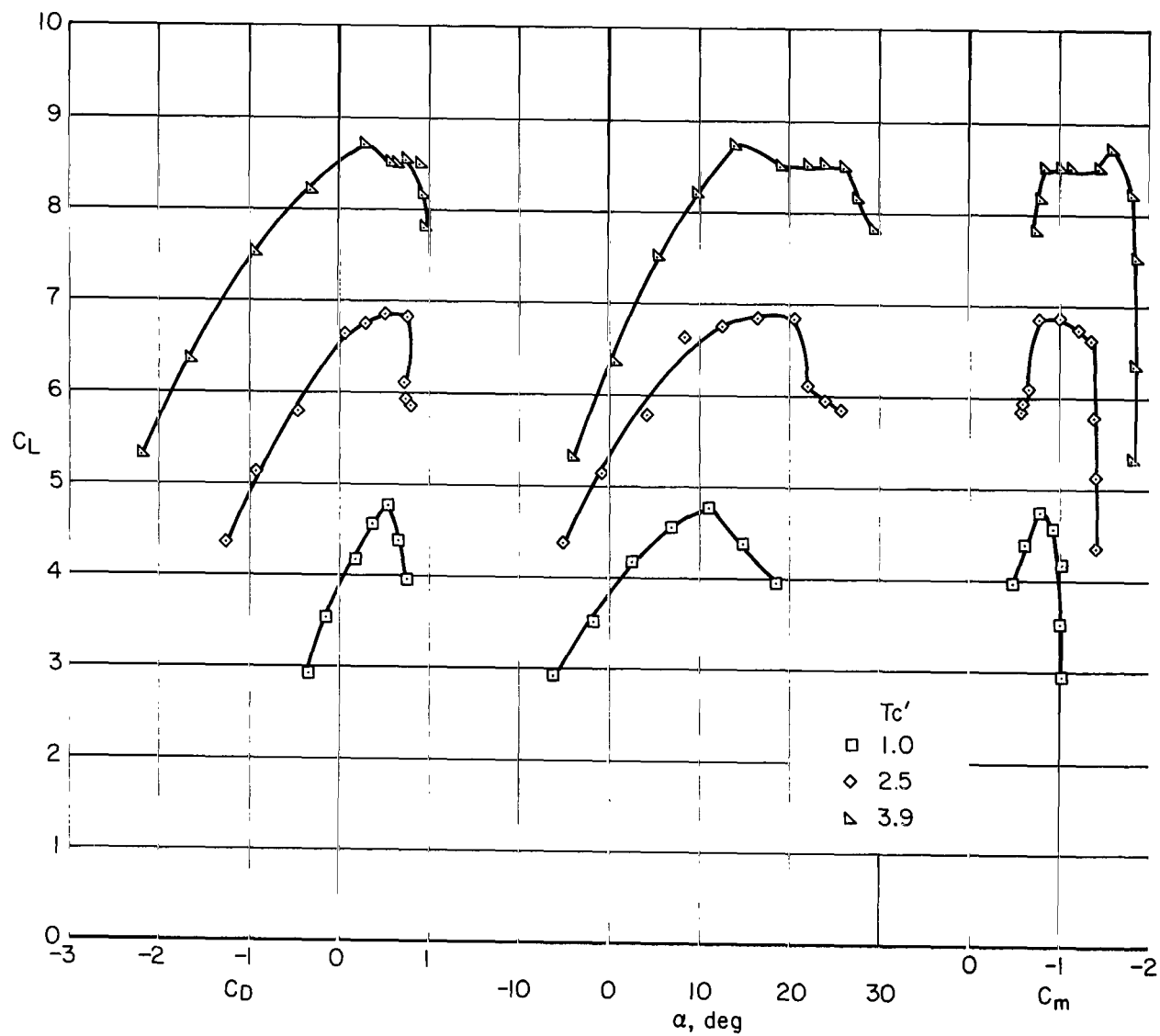
(d) $\delta_f = 40°$, clean leading edge.

Figure 11.- Continued.
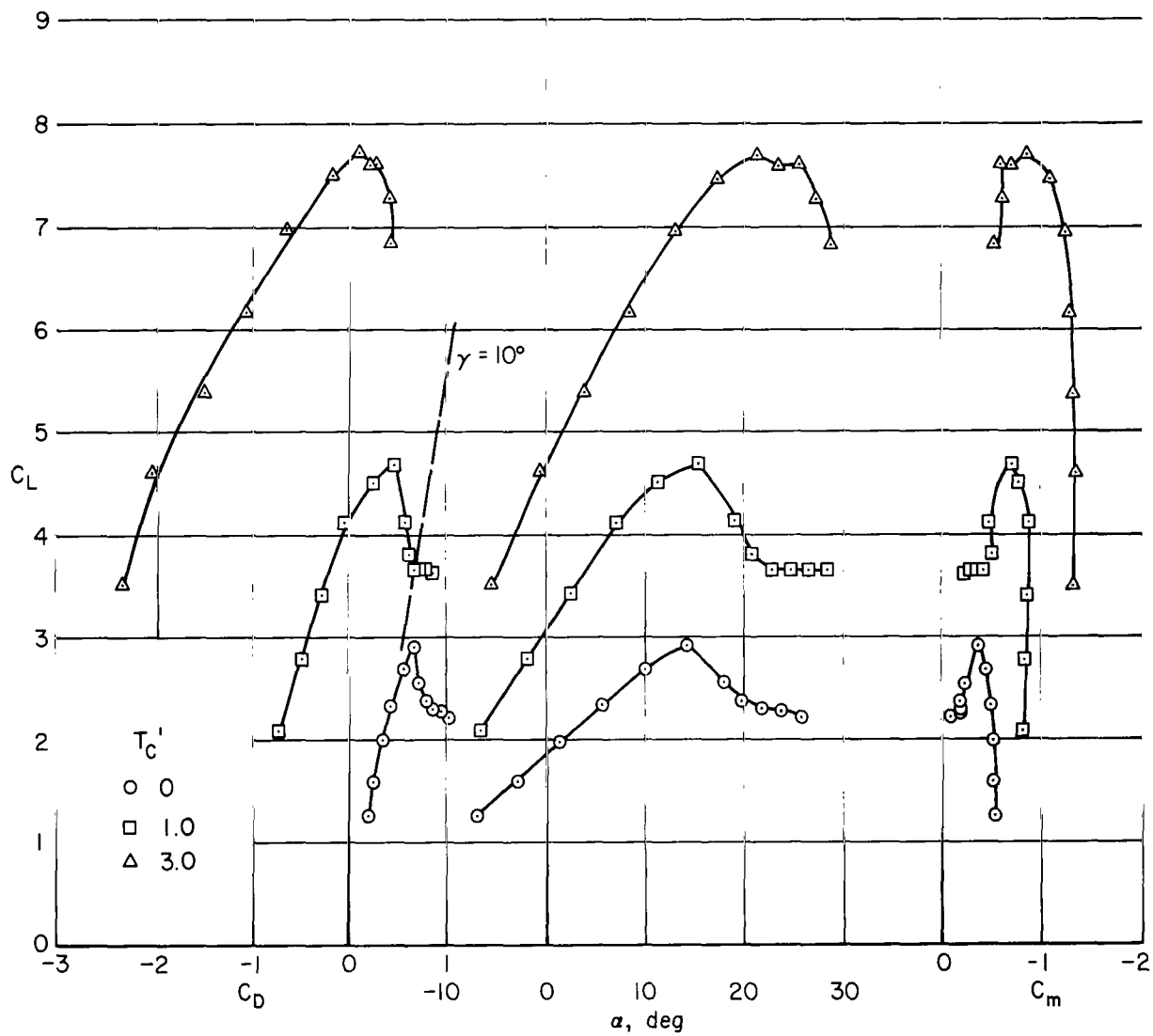
(e) $\delta_f = 60°$, clean leading edge.

Figure 11.- Continued.
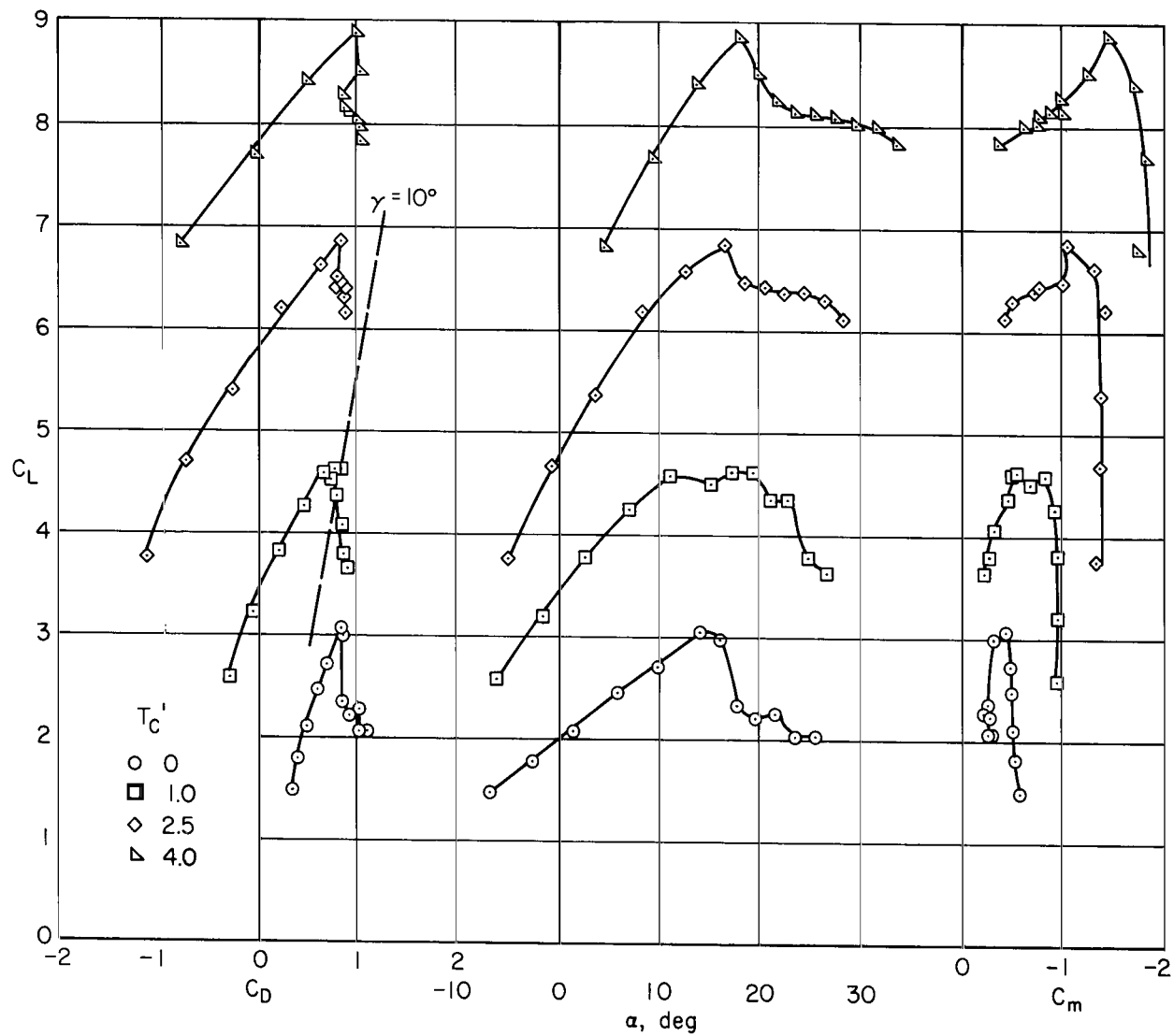
(f) $\delta_f = 80^o$, clean leading edge.

Figure 11.- Continued.
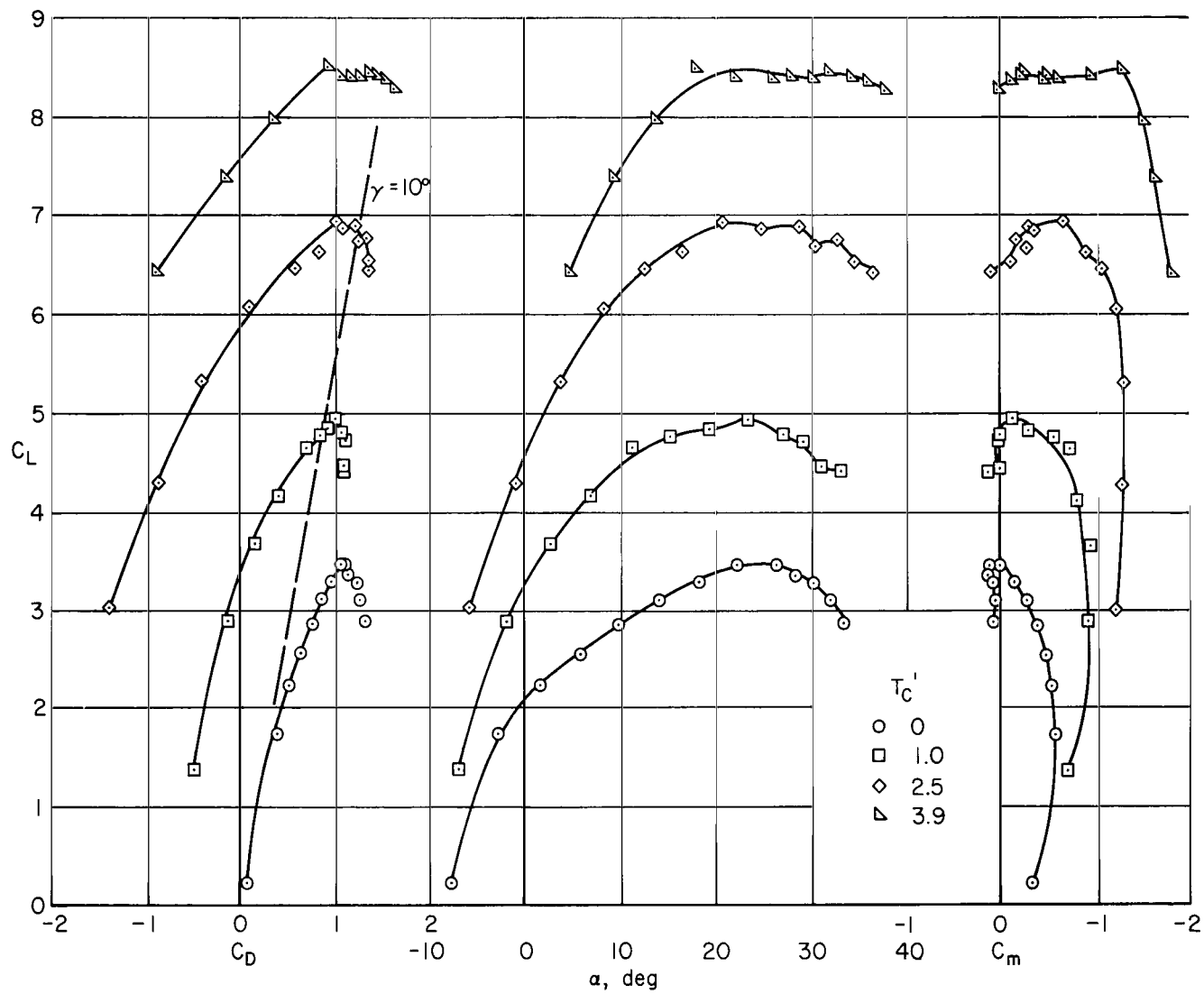
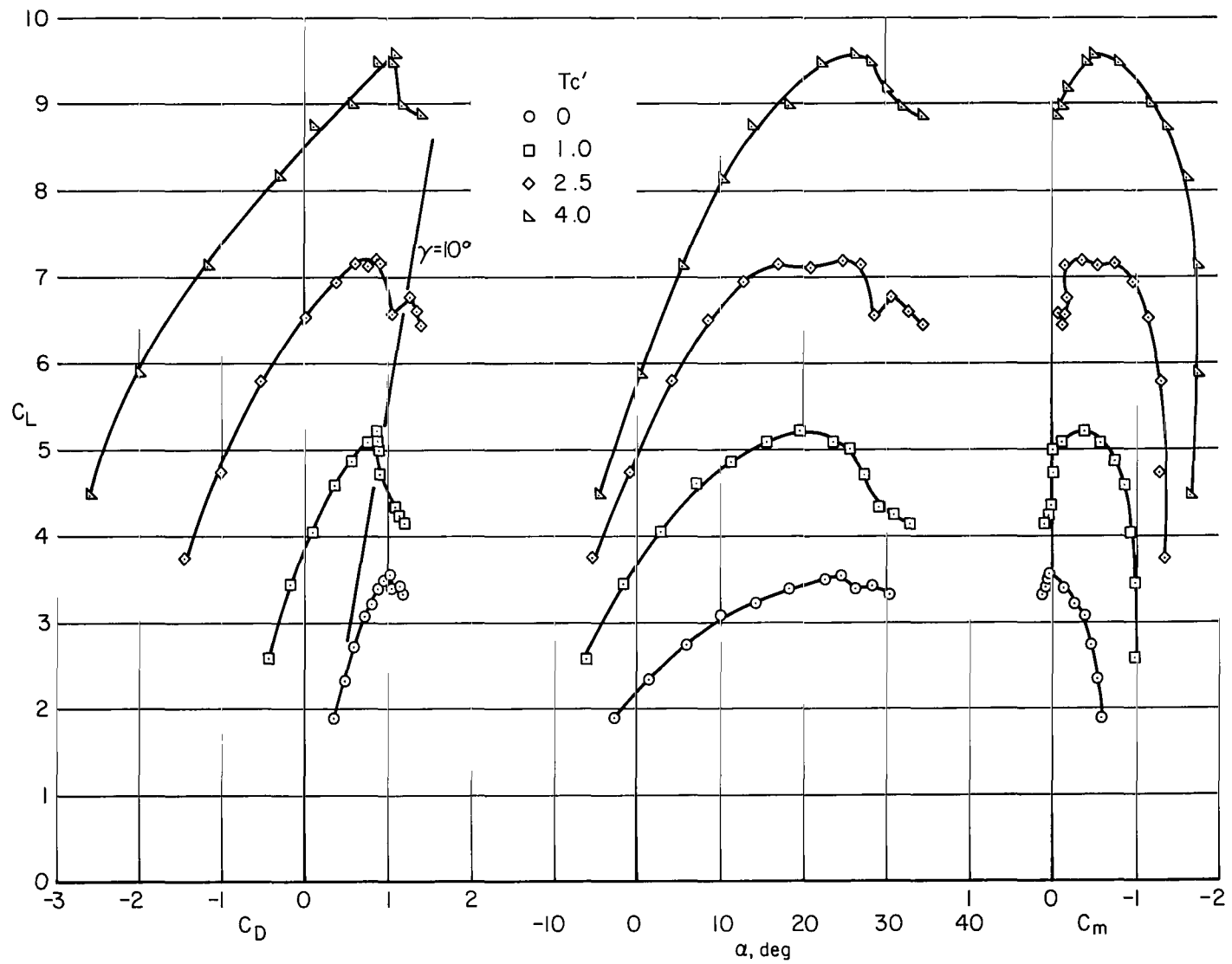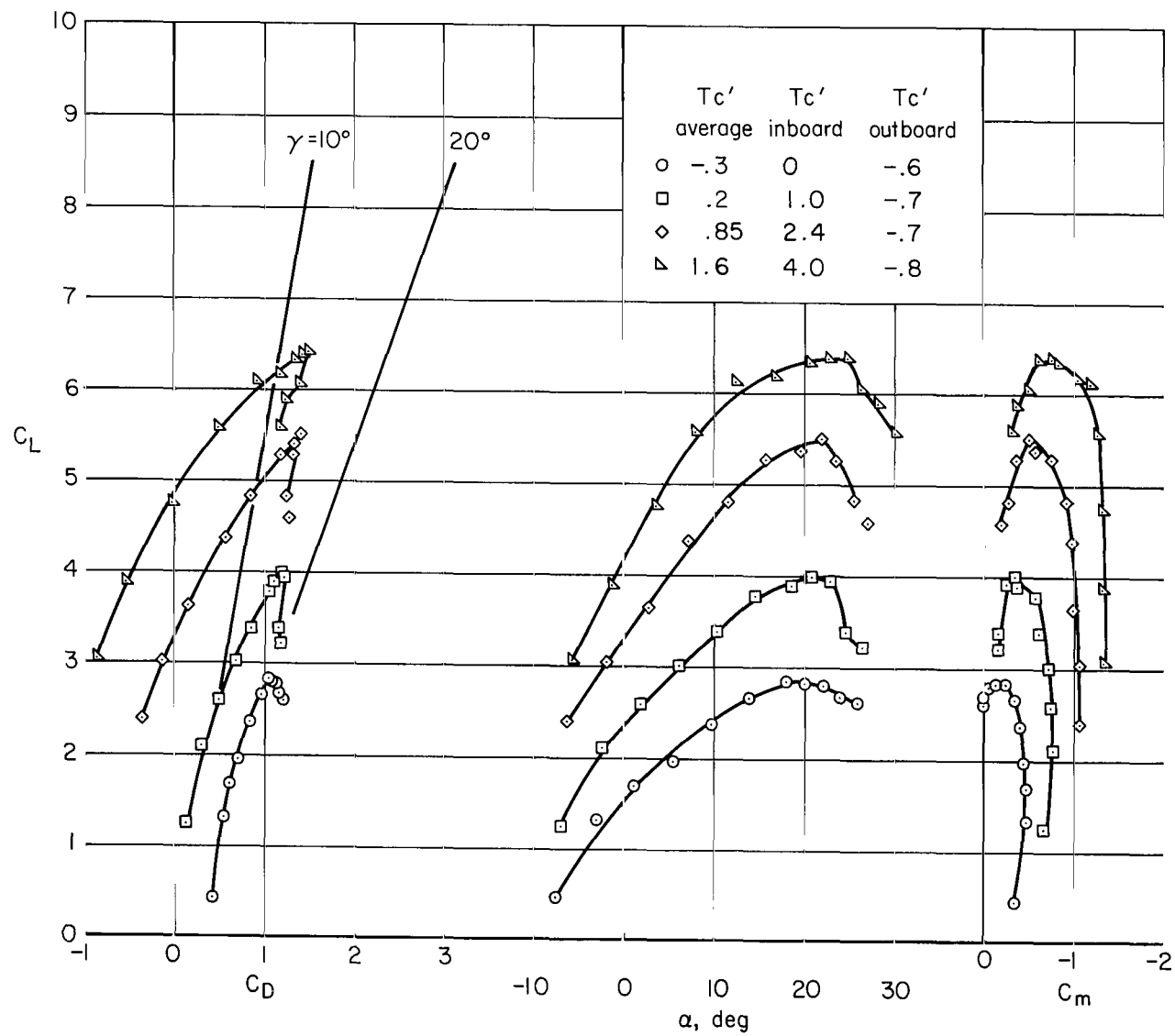(g) $\delta_f = 80°$, full-span slats.

Figure 11.- Continued.
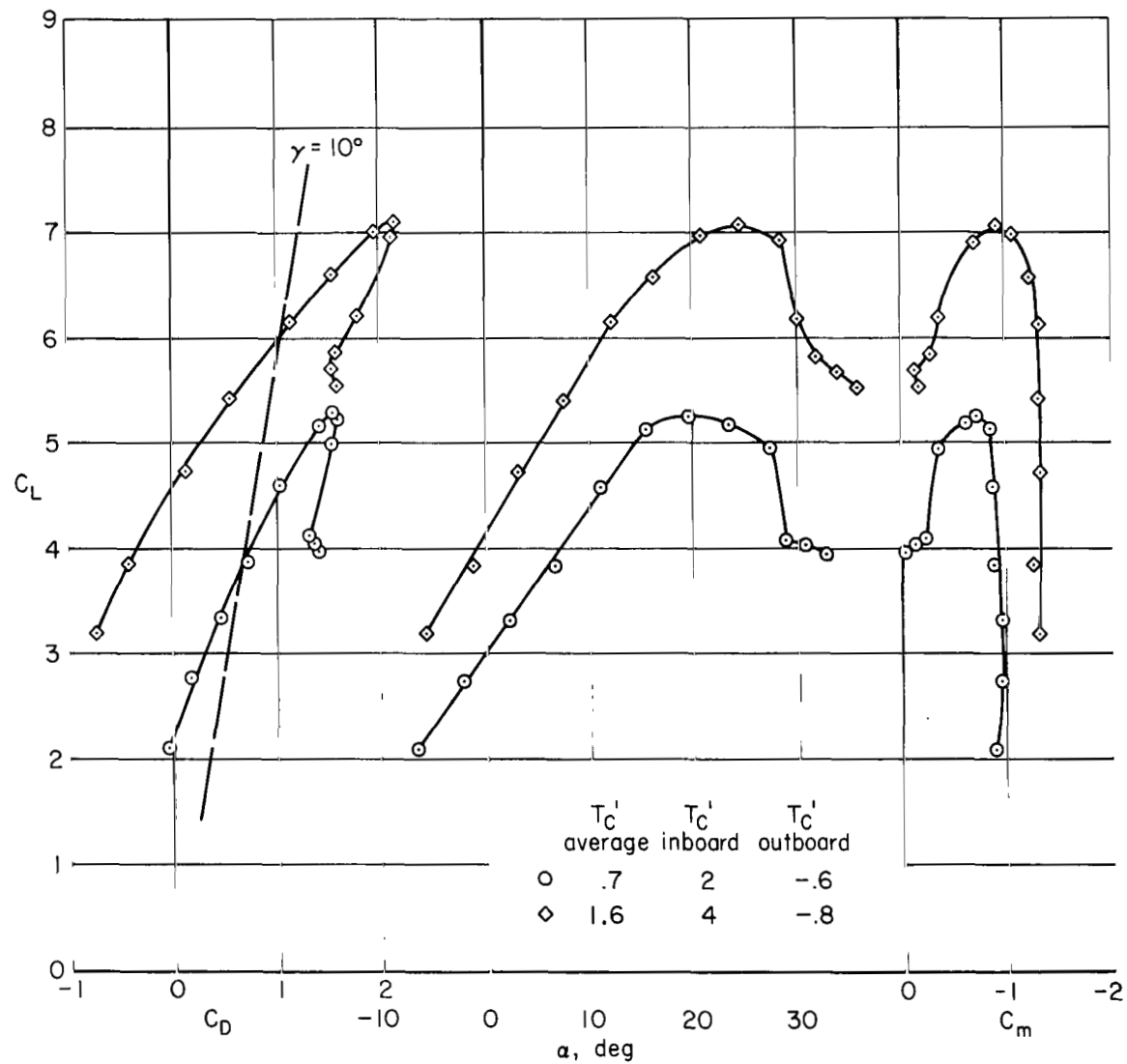
(h) $\delta_f = 80°$, slats outboard of inboard nacelle; $\beta_I = 16°$, $\beta_0 = 0°$.

Figure 11.- Continued.
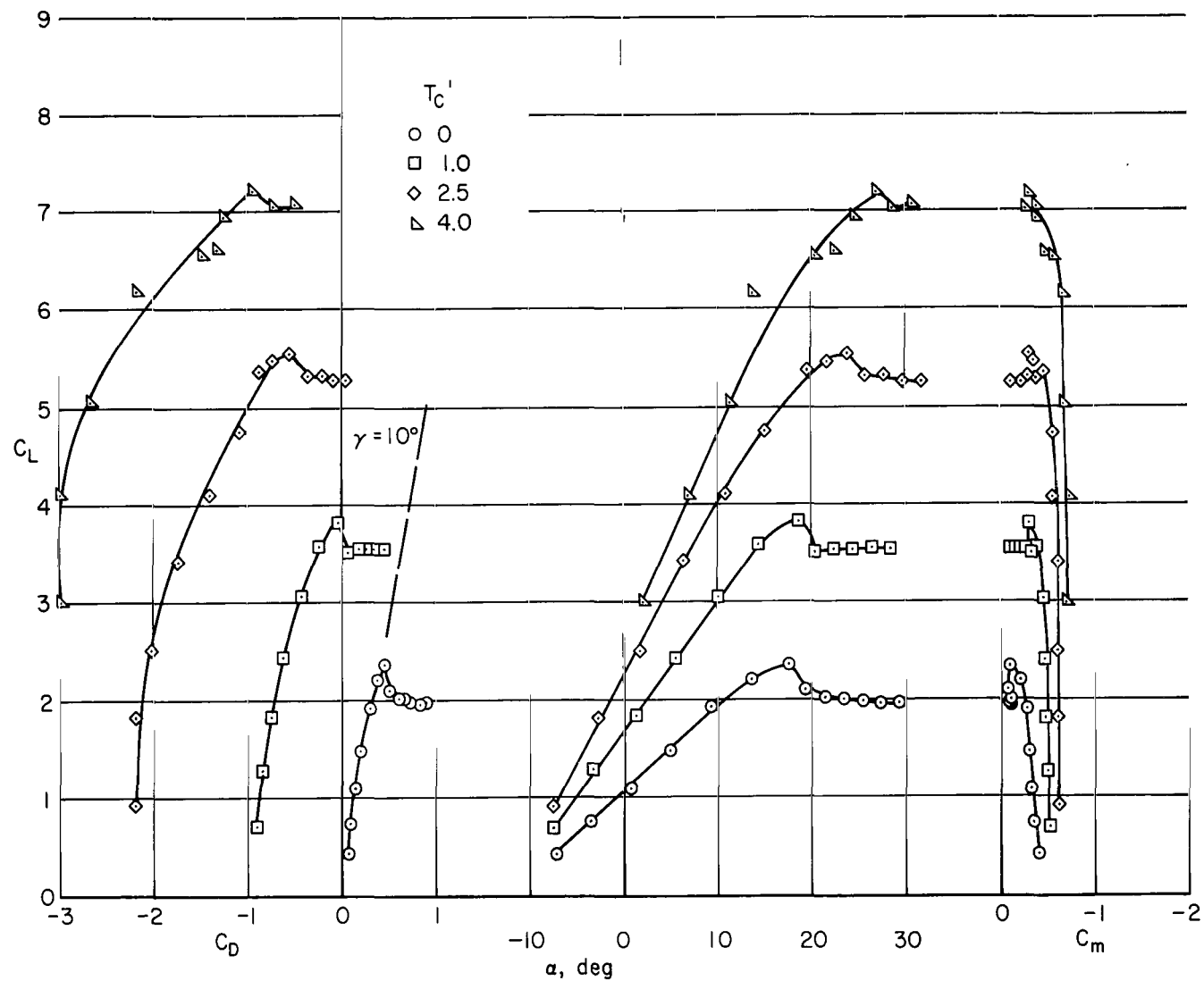
(i) δ_f = 40/20, clean leading edge.

Figure 11.- Continued.
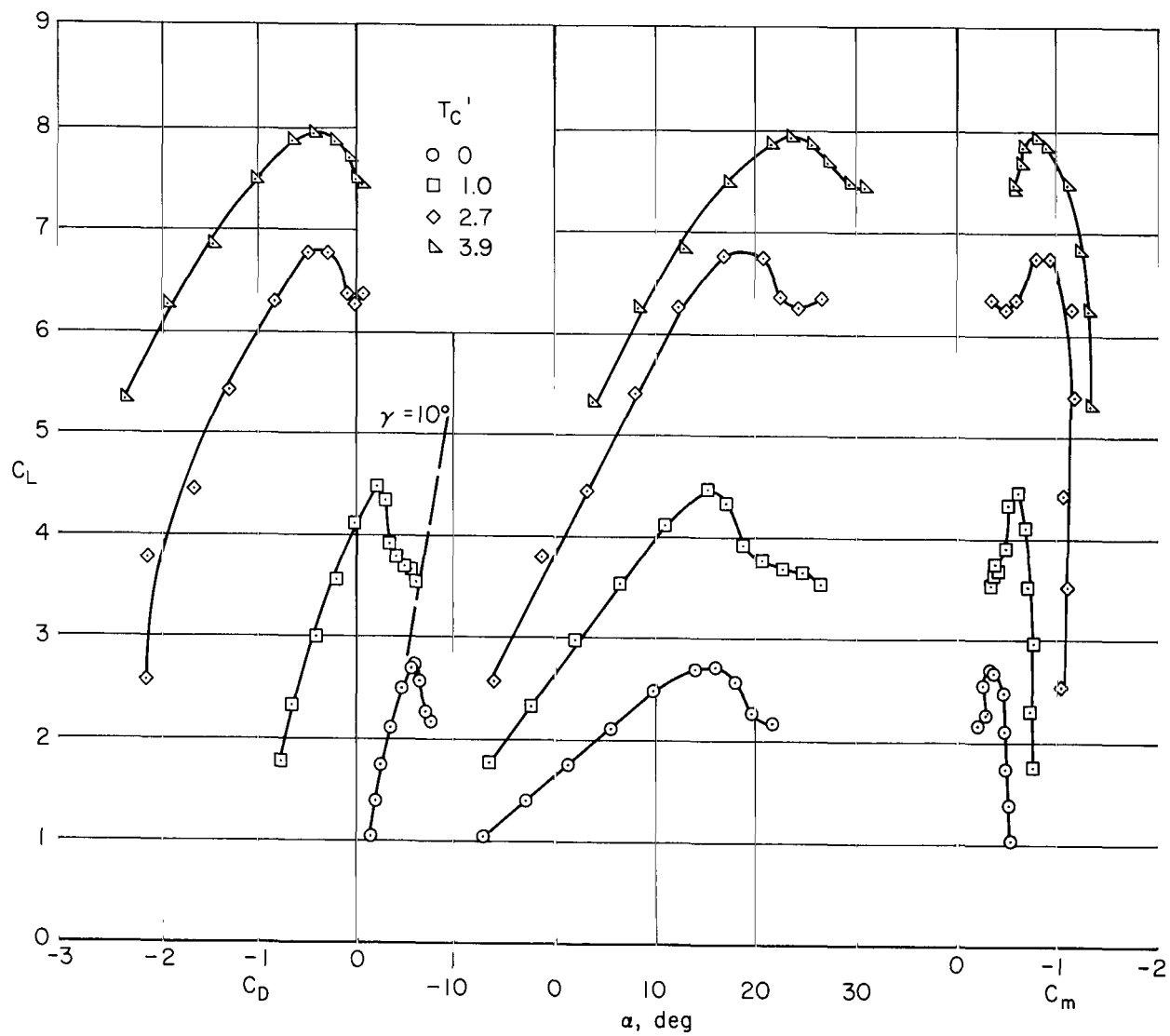
(j) $\delta_f = 60/40$, clean leading edge.

Figure 11.- Continued.
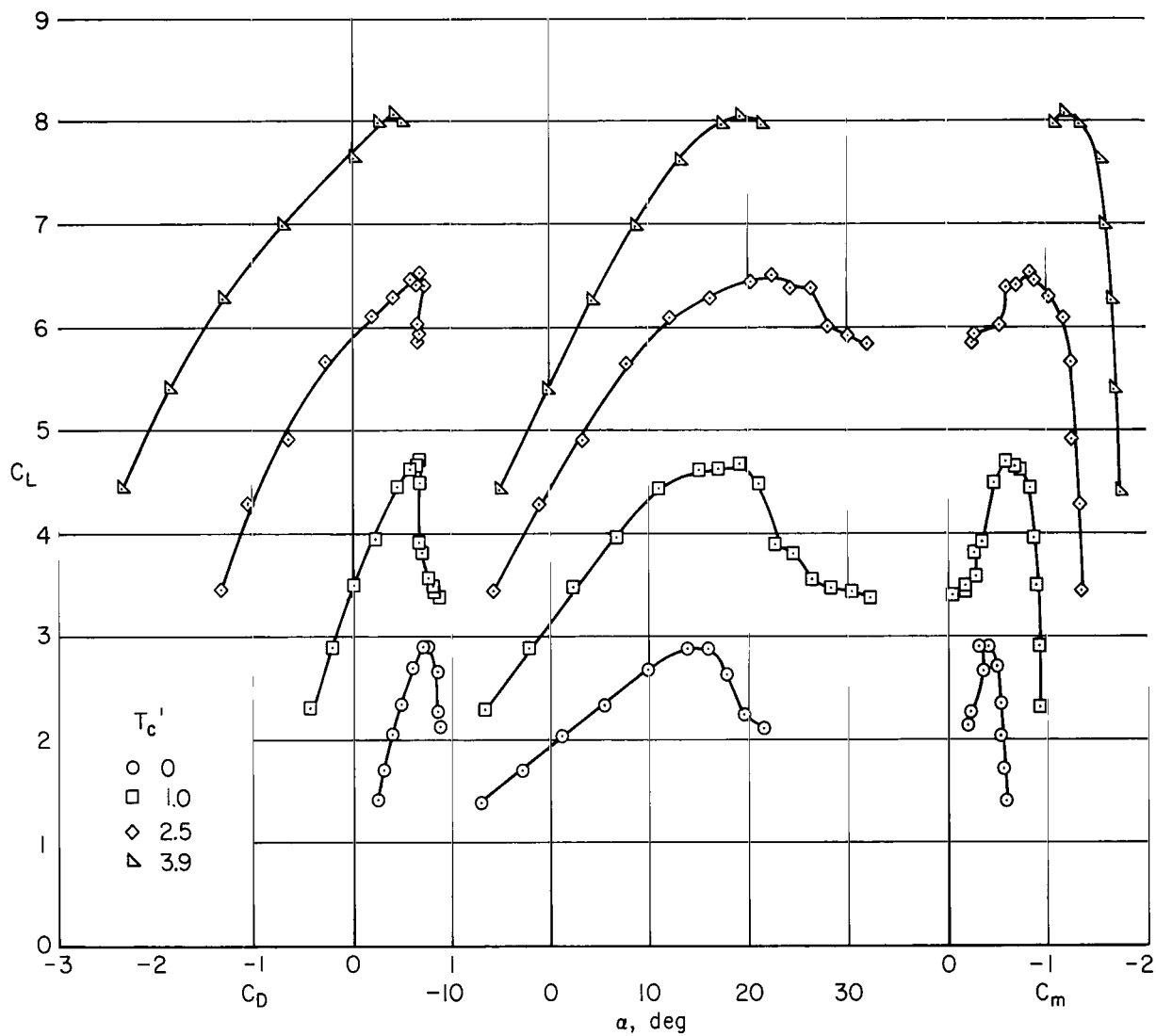
(k) δ_f = 100/60, clean leading edge.

Figure 11.- Concluded.
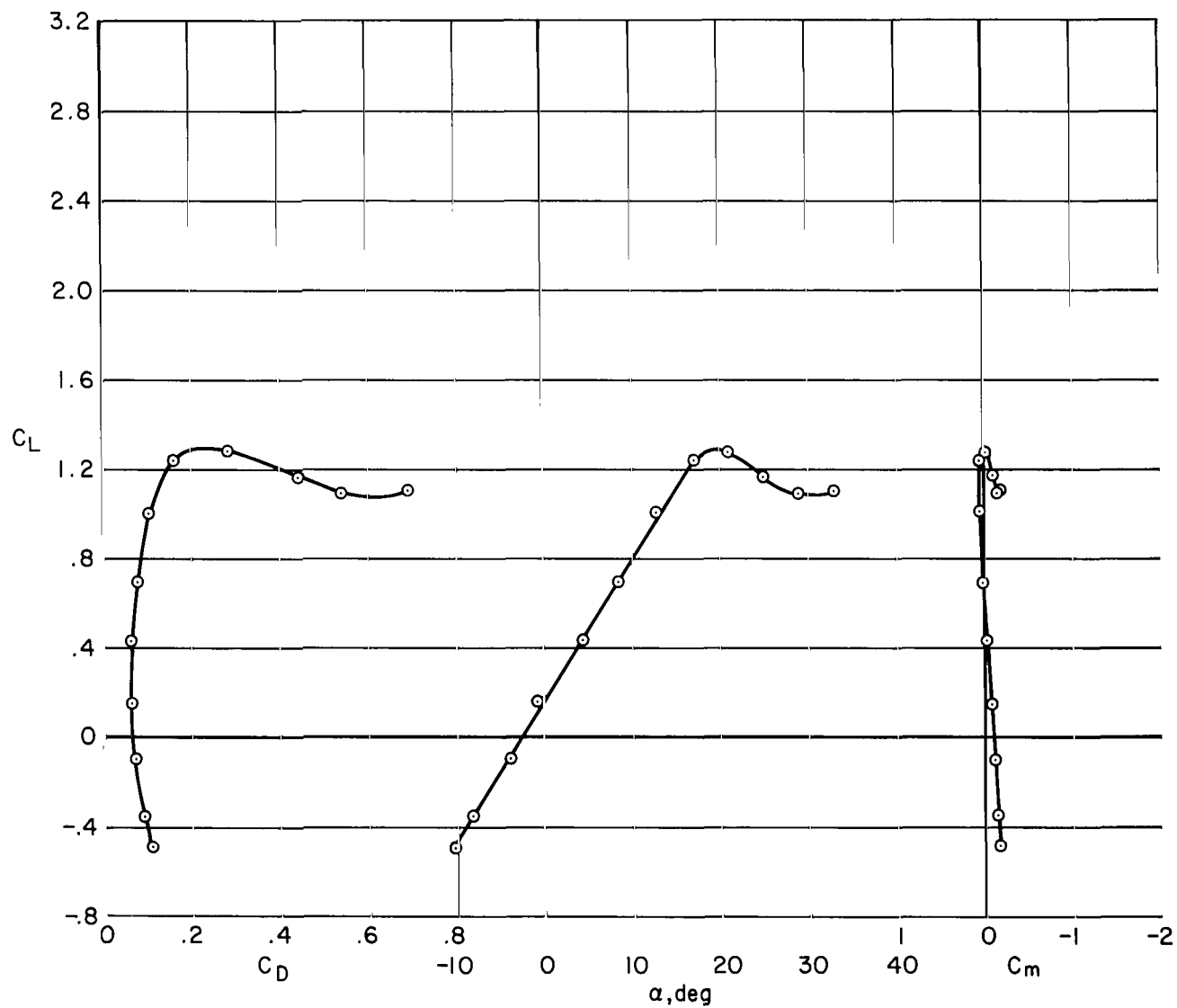
(a) $\delta_f = 0°$, propellers off, clean leading edge.

Figure 12.- Longitudinal characteristics of the model with the medium-span wing; tail off.
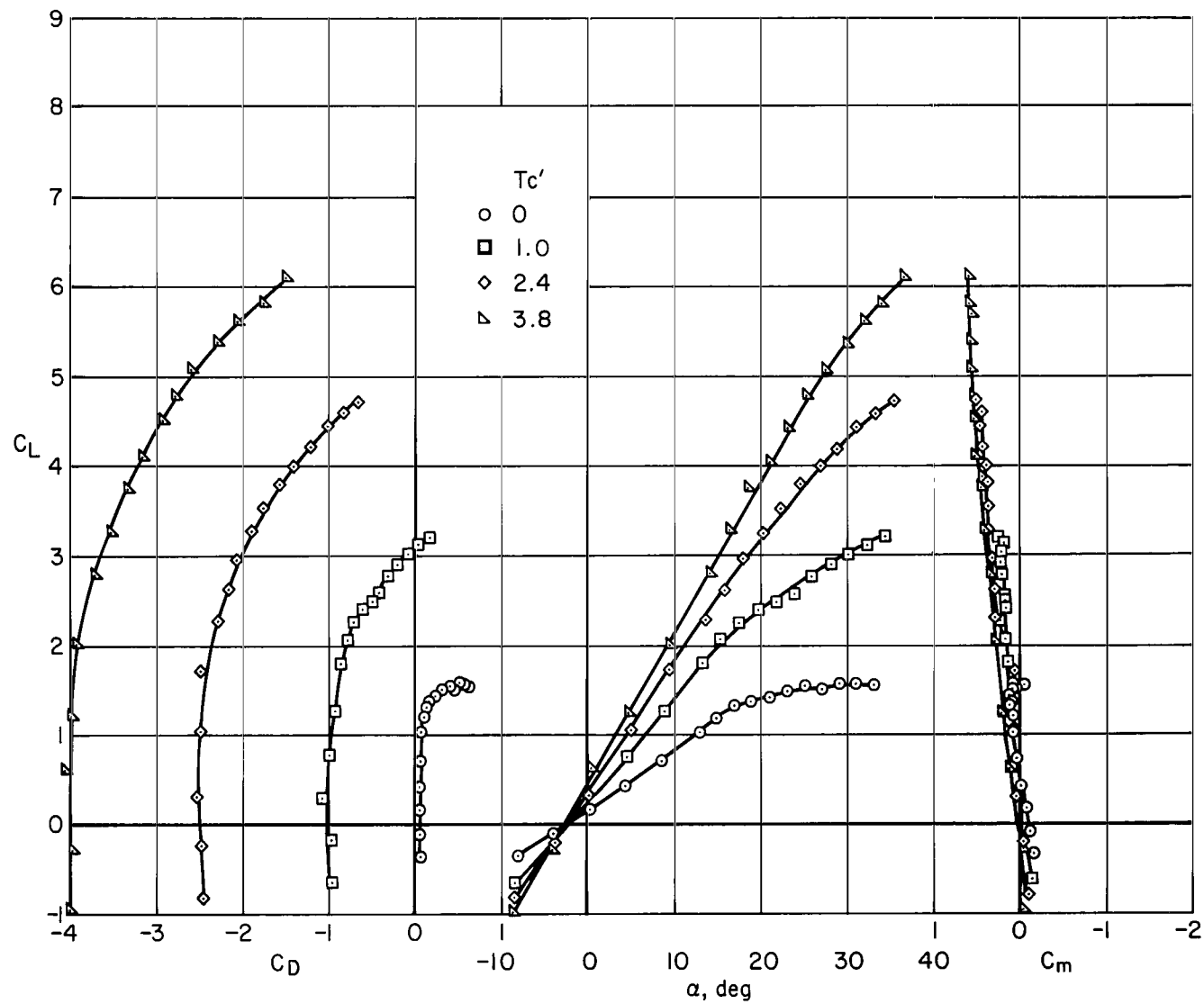
(b) $\delta_f = 0°$, clean leading edge.

Figure 12.- Continued.
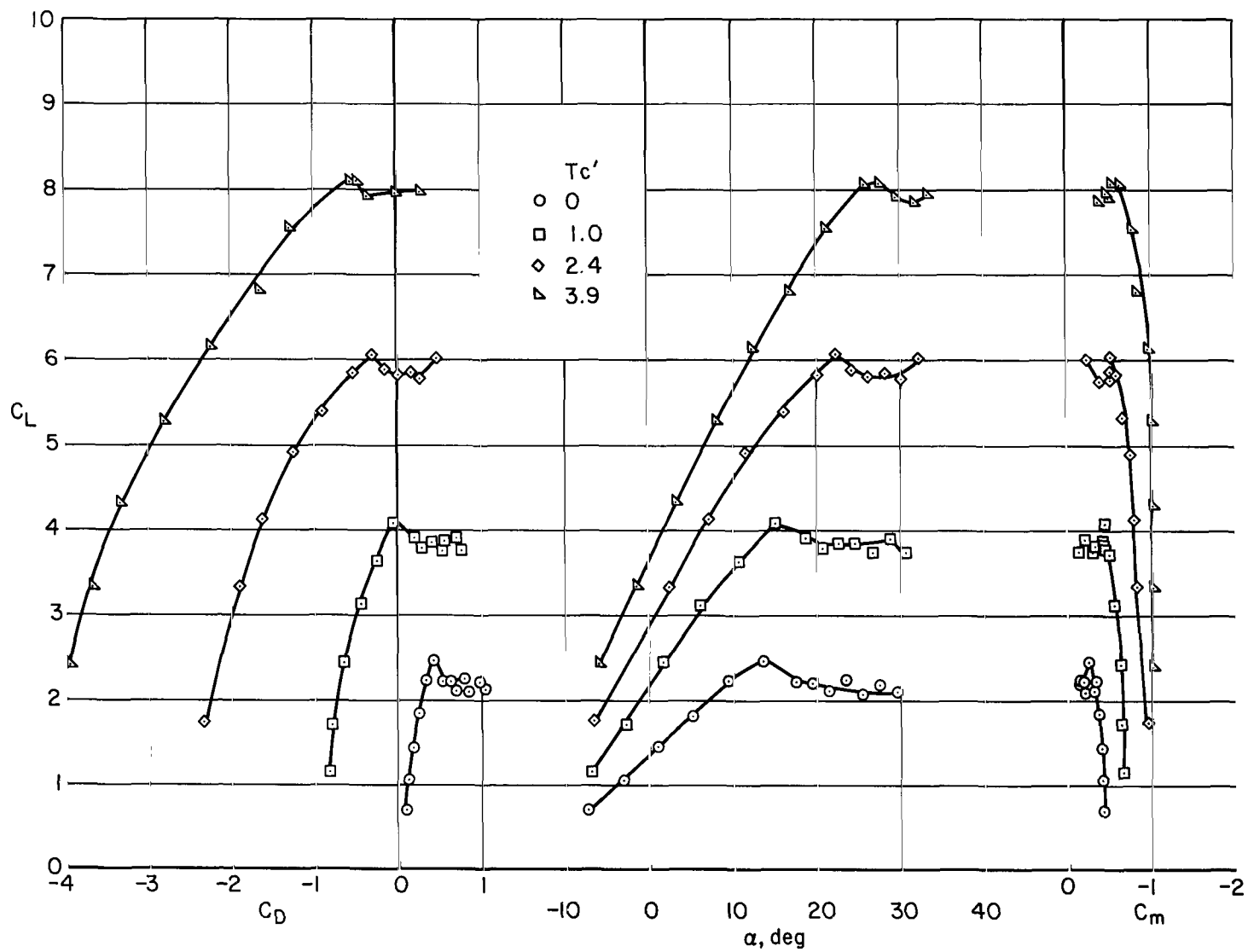
(c) $\delta_f = 40°$, clean leading edge.

Figure 12.- Continued.

(d) $\delta_f = 40°$, full-span slats.

Figure 12.- Continued.

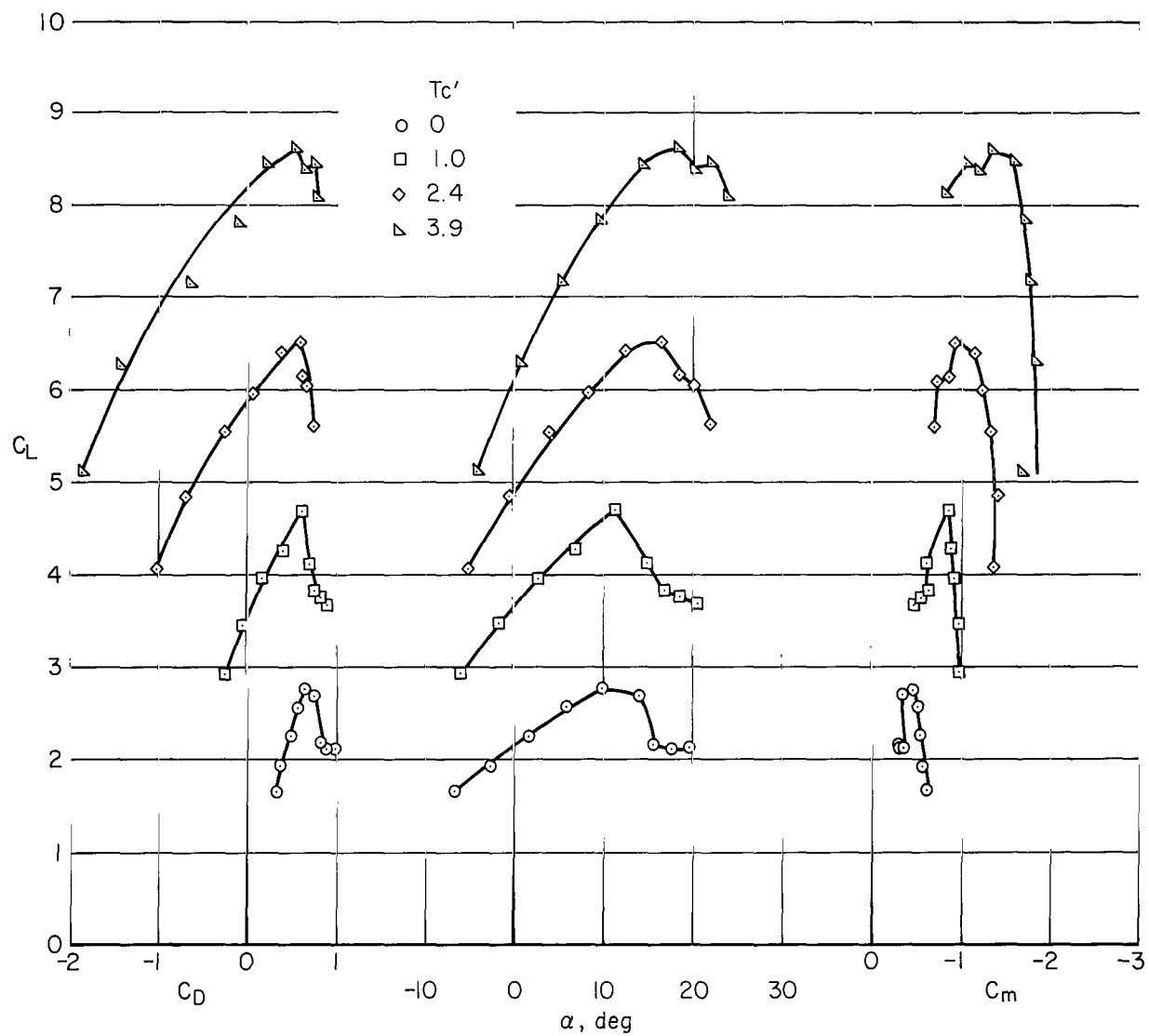(e) $\delta_f = 80^\circ$, clean leading edge.

Figure 12.- Continued.

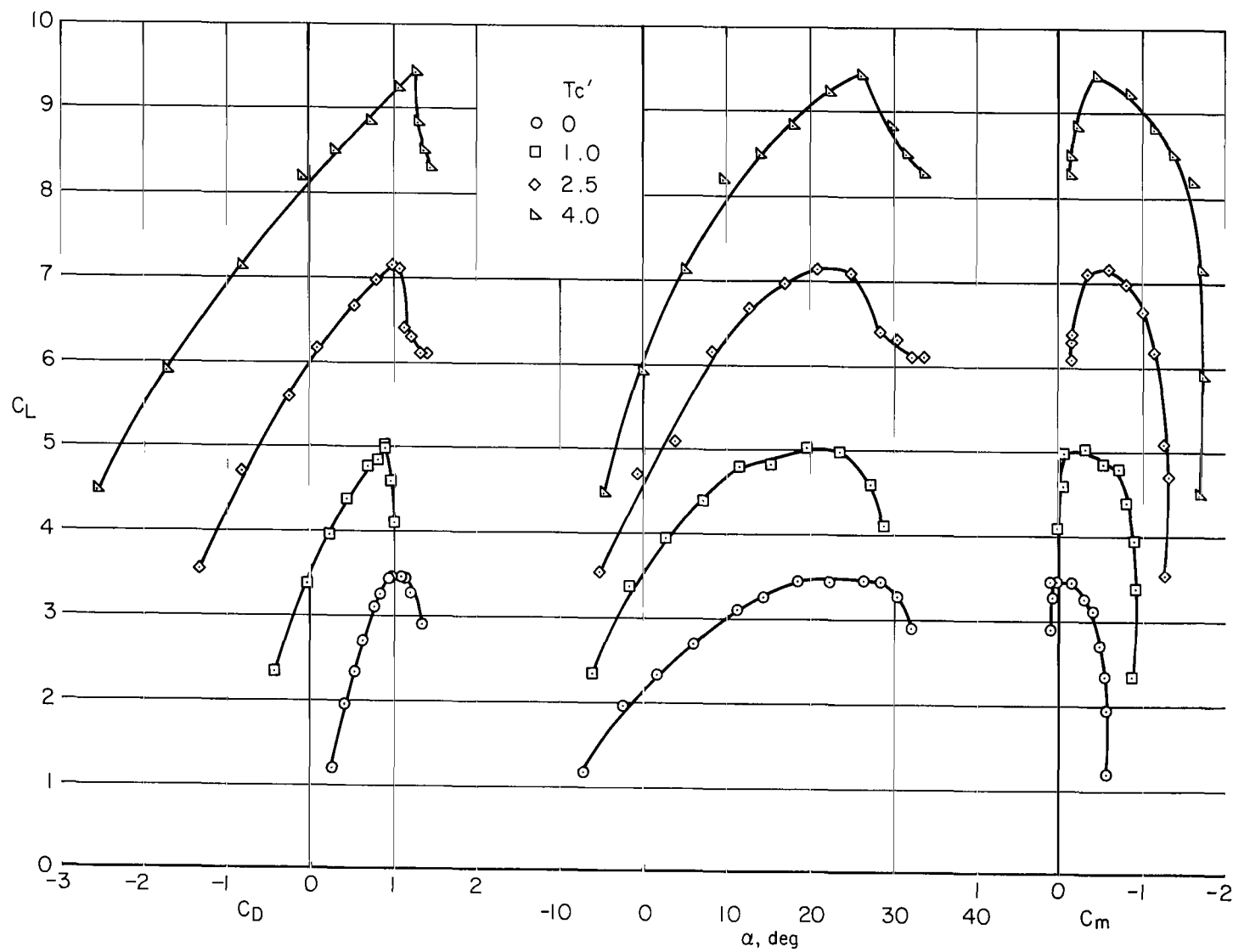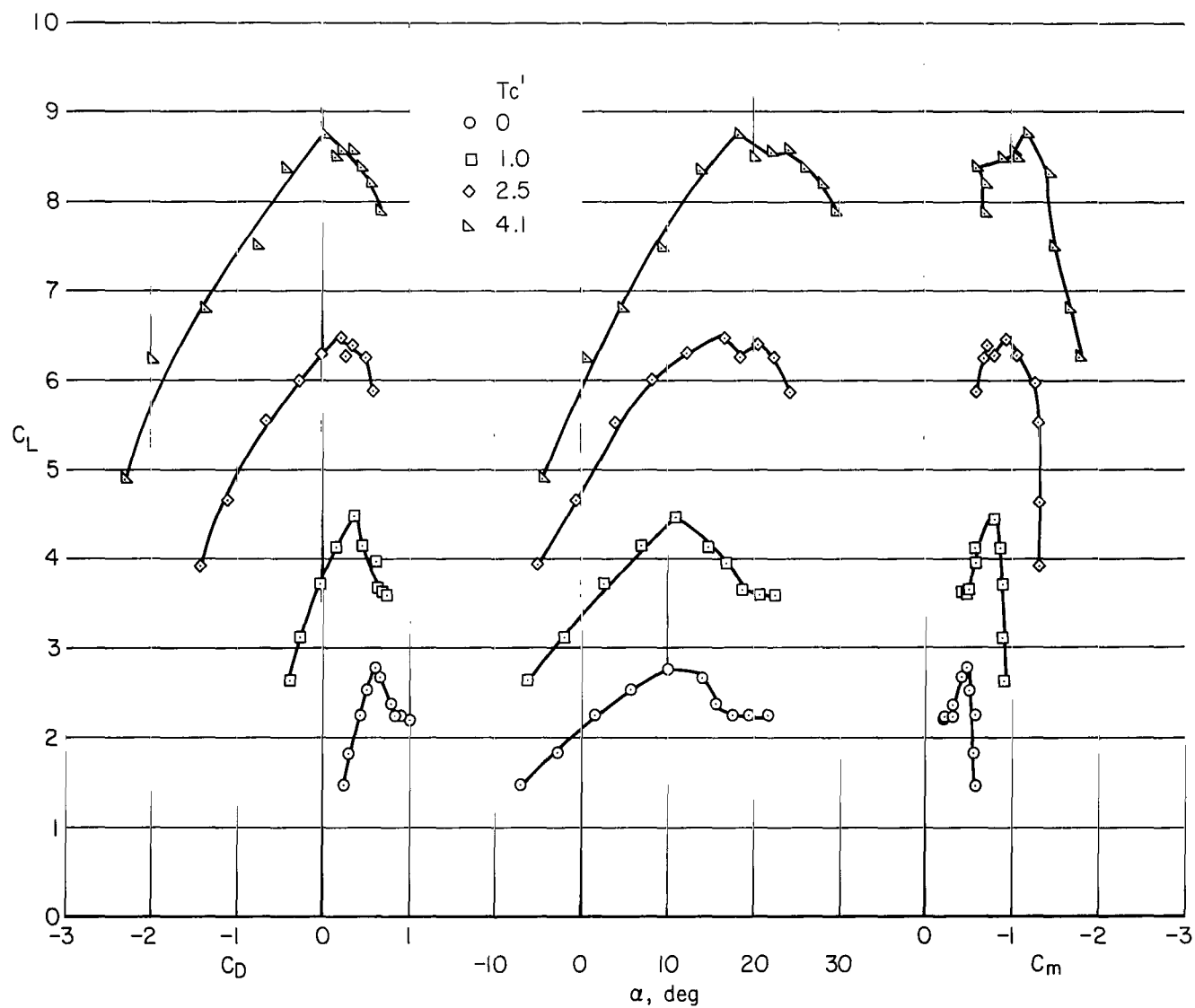(f) $\delta_f = 80^\circ$, full-span slats.

Figure 12.- Continued.

	Tc' average	Tc' inboard	Tc' outboard
○	−.3	0	−.6
□	.2	1.0	−.7
◇	.85	2.4	−.7
◁	1.6	4.0	−.8

(g) $\delta_f = 80°$, full-span slats, $\beta_I = 16°$, $\beta_0 = 0°$.

Figure 12.- Continued.

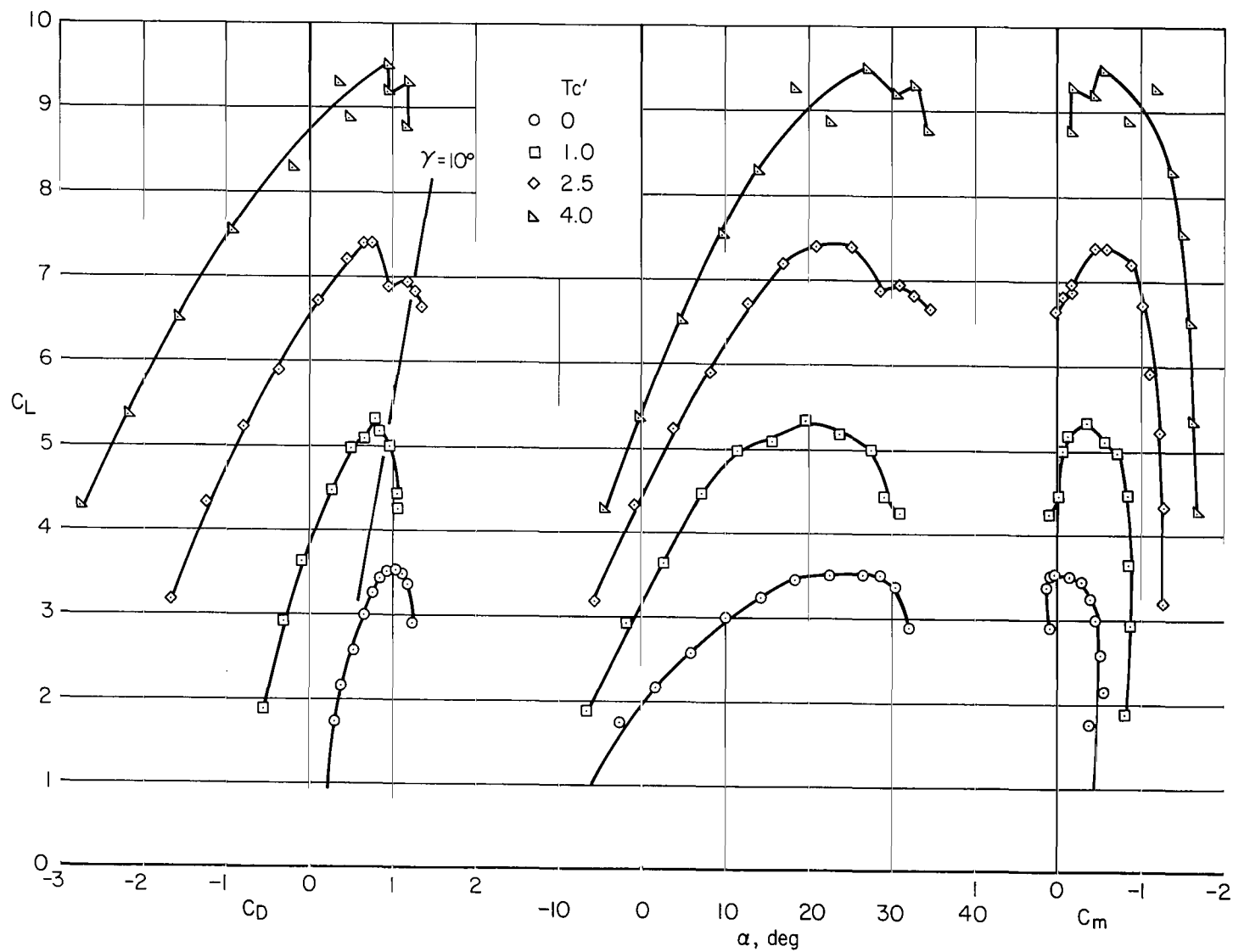(h) $\delta_f = 100^\circ$, clean leading edge.

Figure 12.- Continued.

(i) $\delta_f = 100^\circ$, full-span slats.

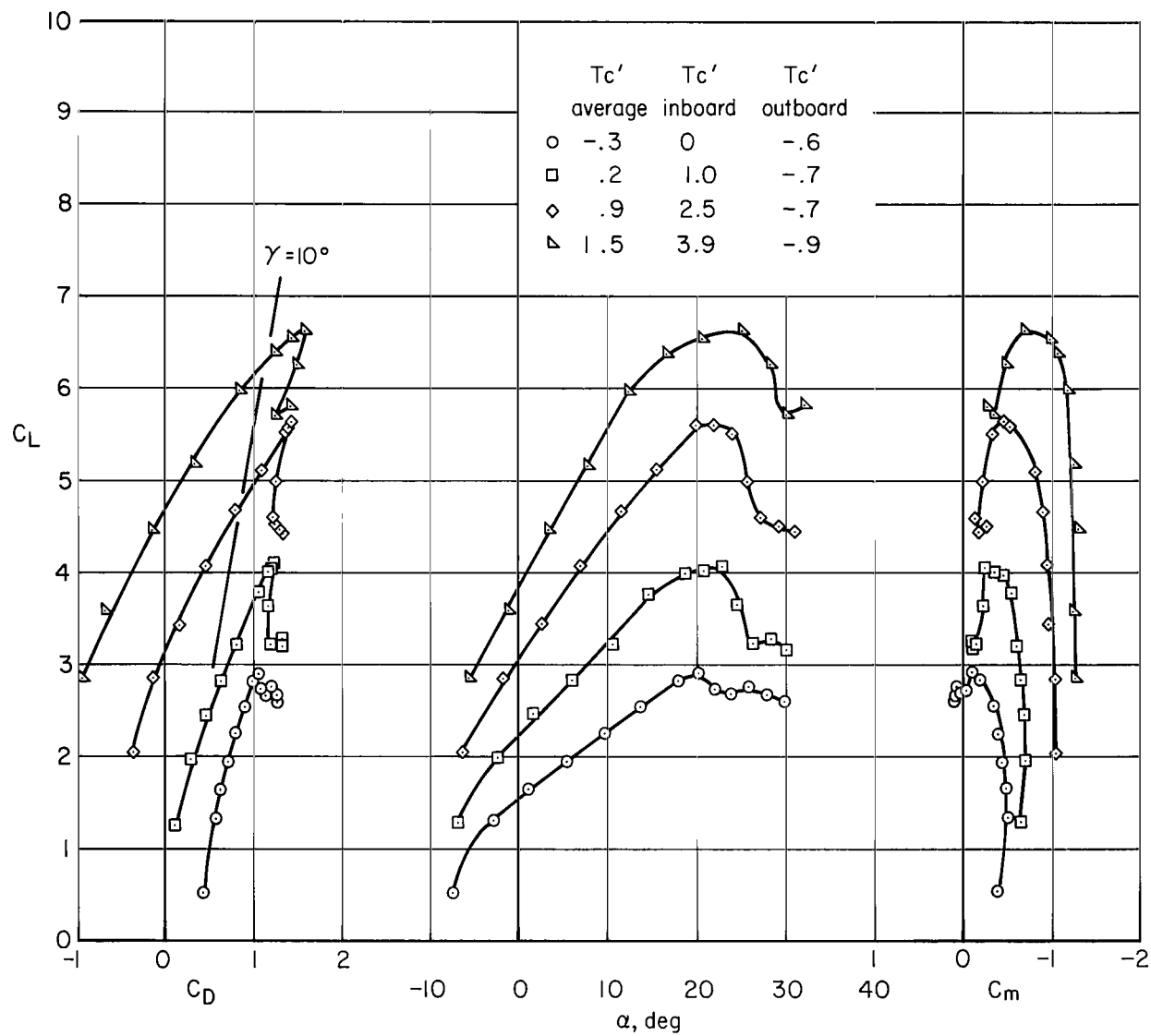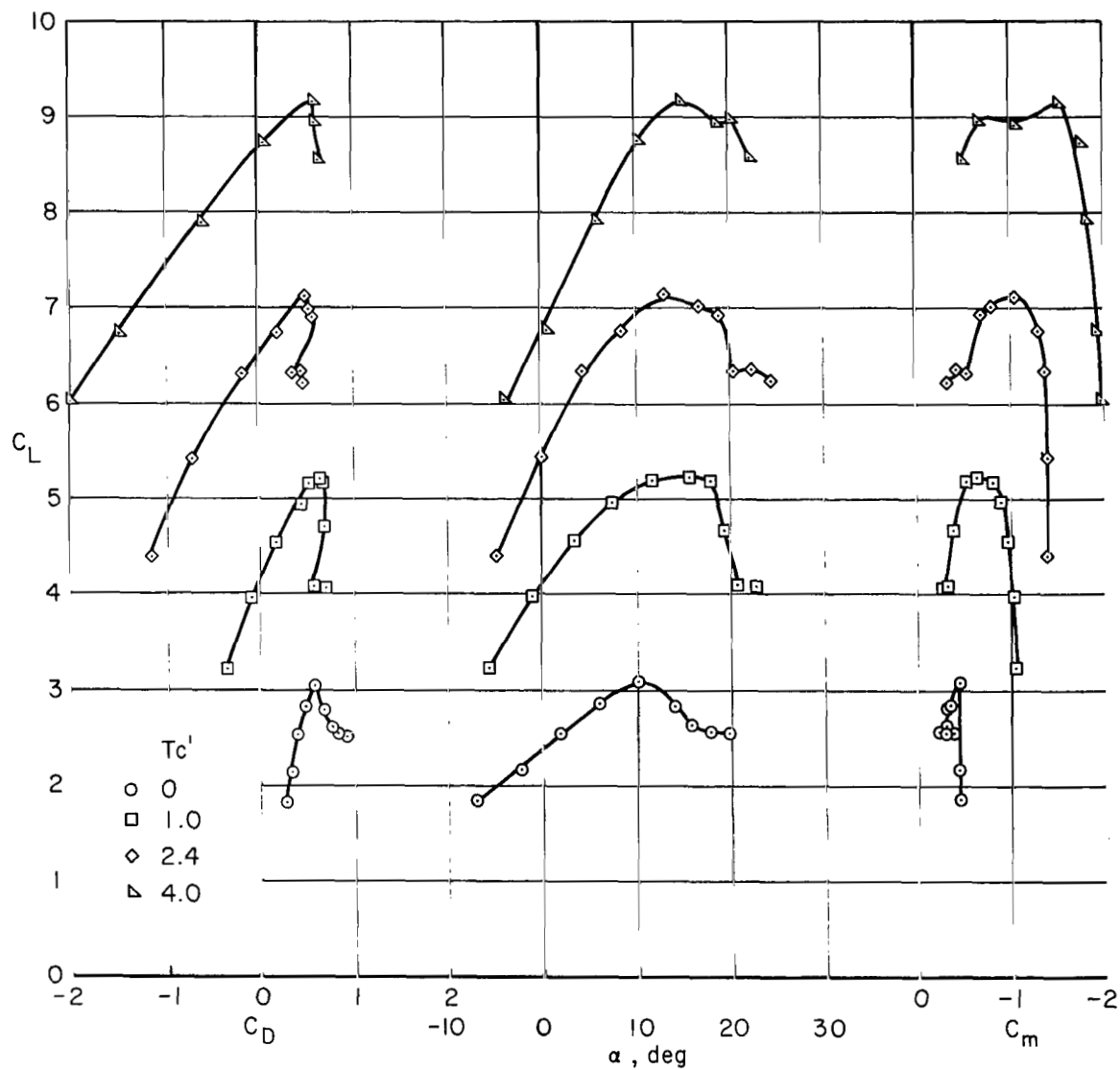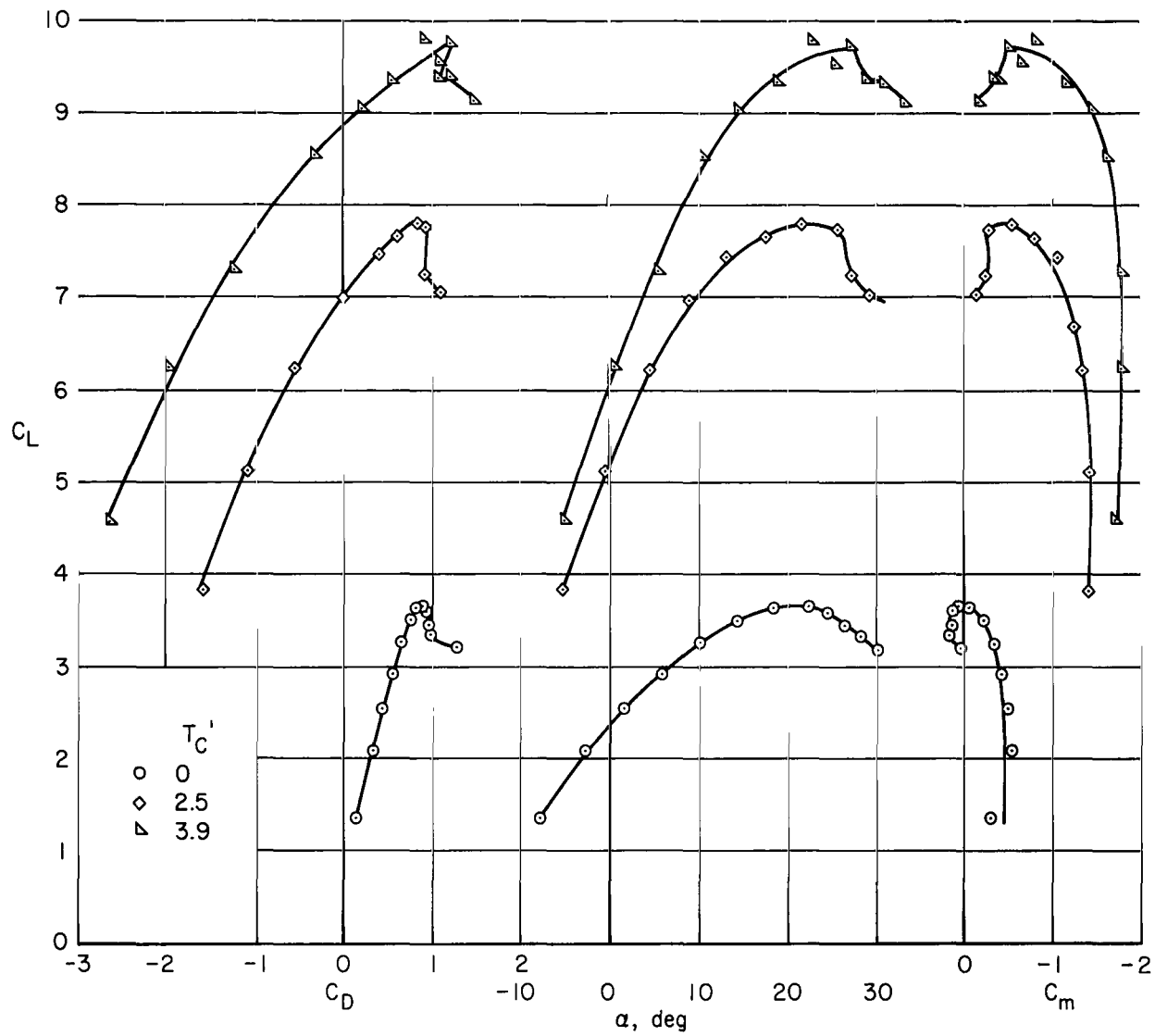Figure 12.- Continued.

(j) $\delta_f = 100/60$, clean leading edge.

Figure 12.- Continued.

10

9

8

7

6

C_L

5

4

3

2

1

0

Tc′

○ 0
□ 1.0
◇ 2.5
◁ 4.0

$\gamma = 10°$

-3   -2   -1   0   1   2

C_D

-10   0   10   20   30   40

α, deg

0   -1   -2

C_m

(k) $\delta_f = 100/60$, full-span slats.

Figure 12.- Continued.

$$(l) \quad \delta_f = 100/60, \text{ full-span slats}, \beta_I = 16^o, \beta_0 = 0^o.$$
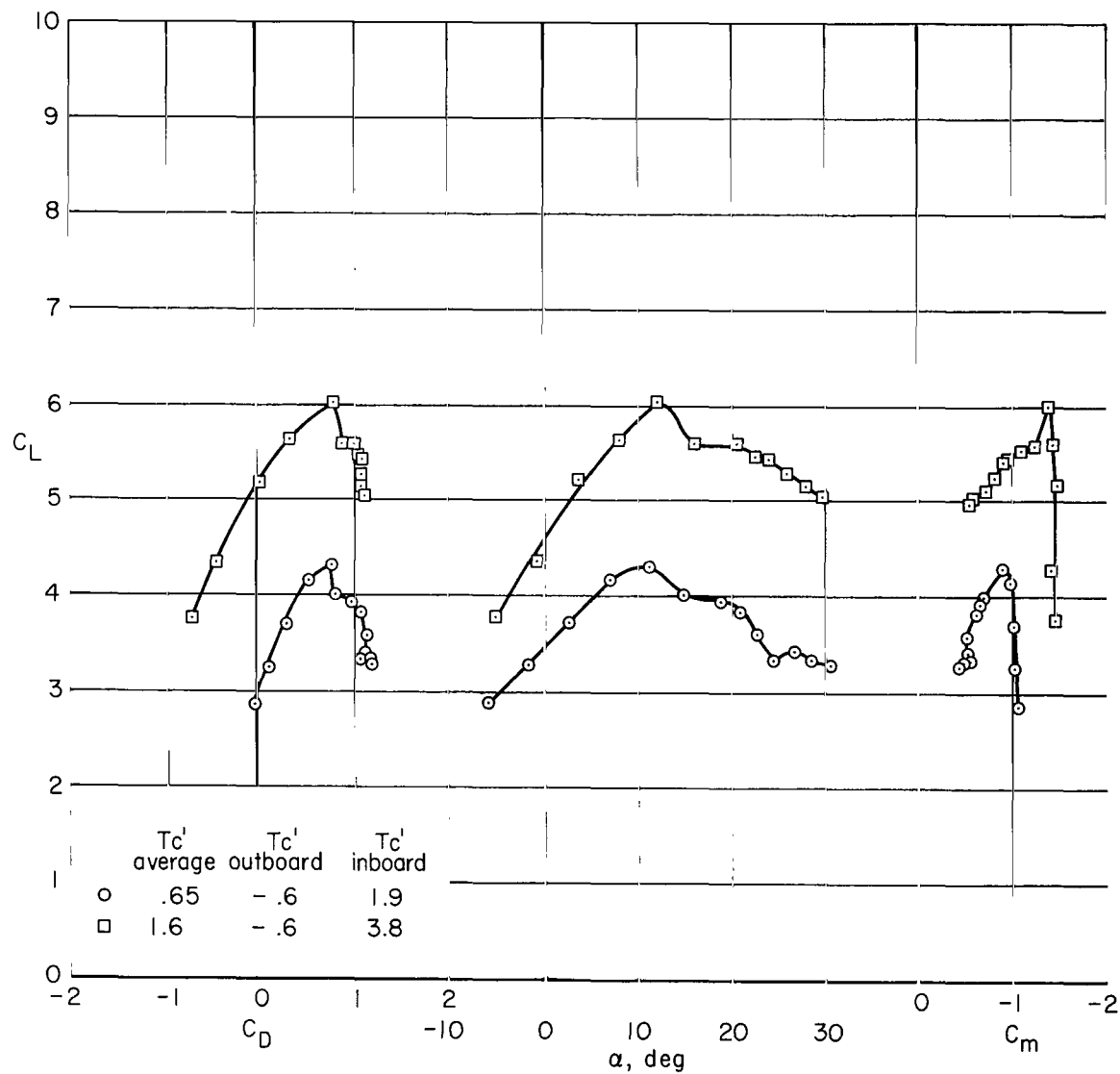
Figure 12.- Concluded.

(a) $\delta_f = 80°$, clean leading edge.

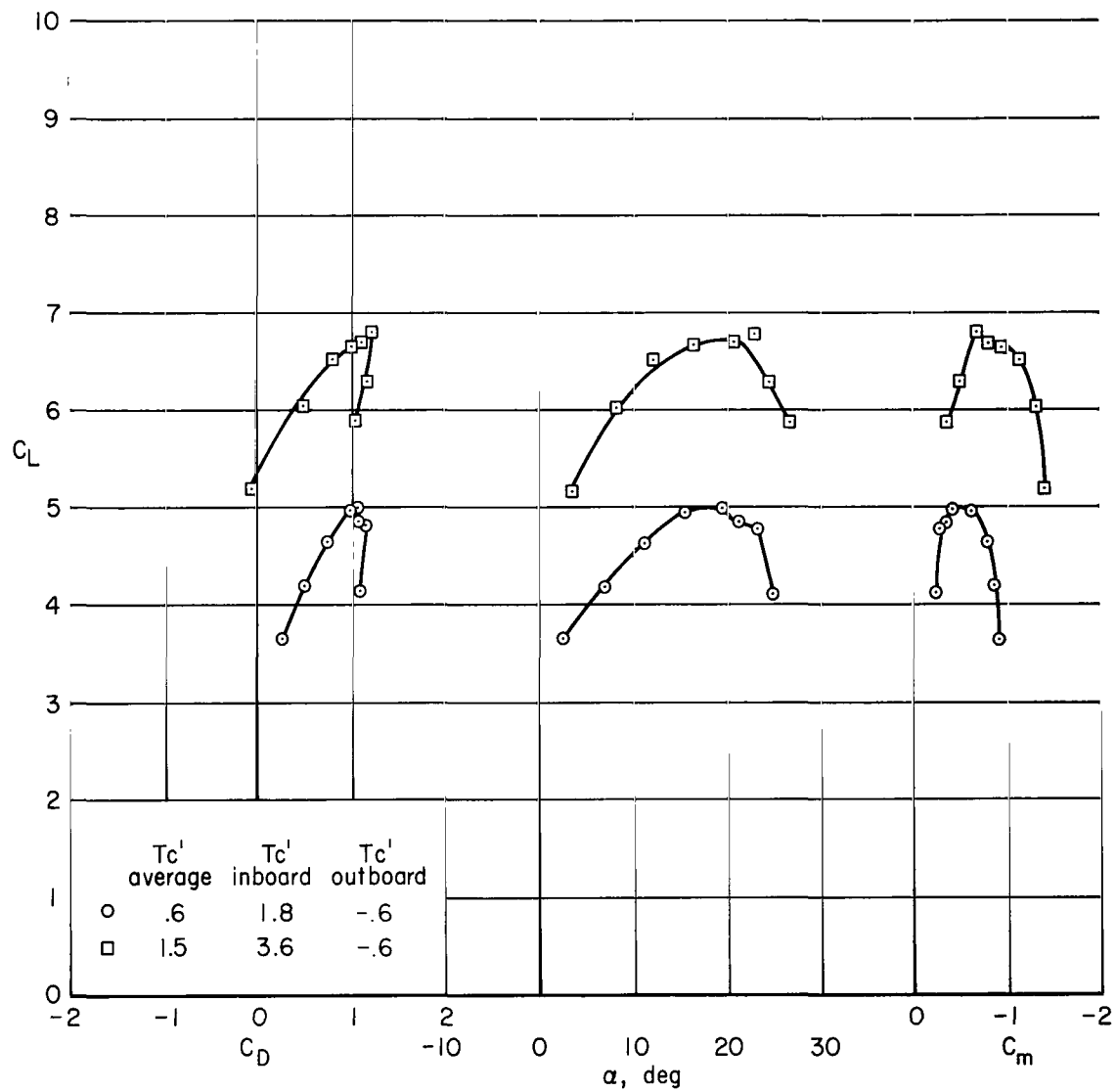Figure 13.- Longitudinal characteristics of the model with the long span wing; tail off.

(b) $\delta_f = 80°$, full-span slats.

Figure 13.- Continued.

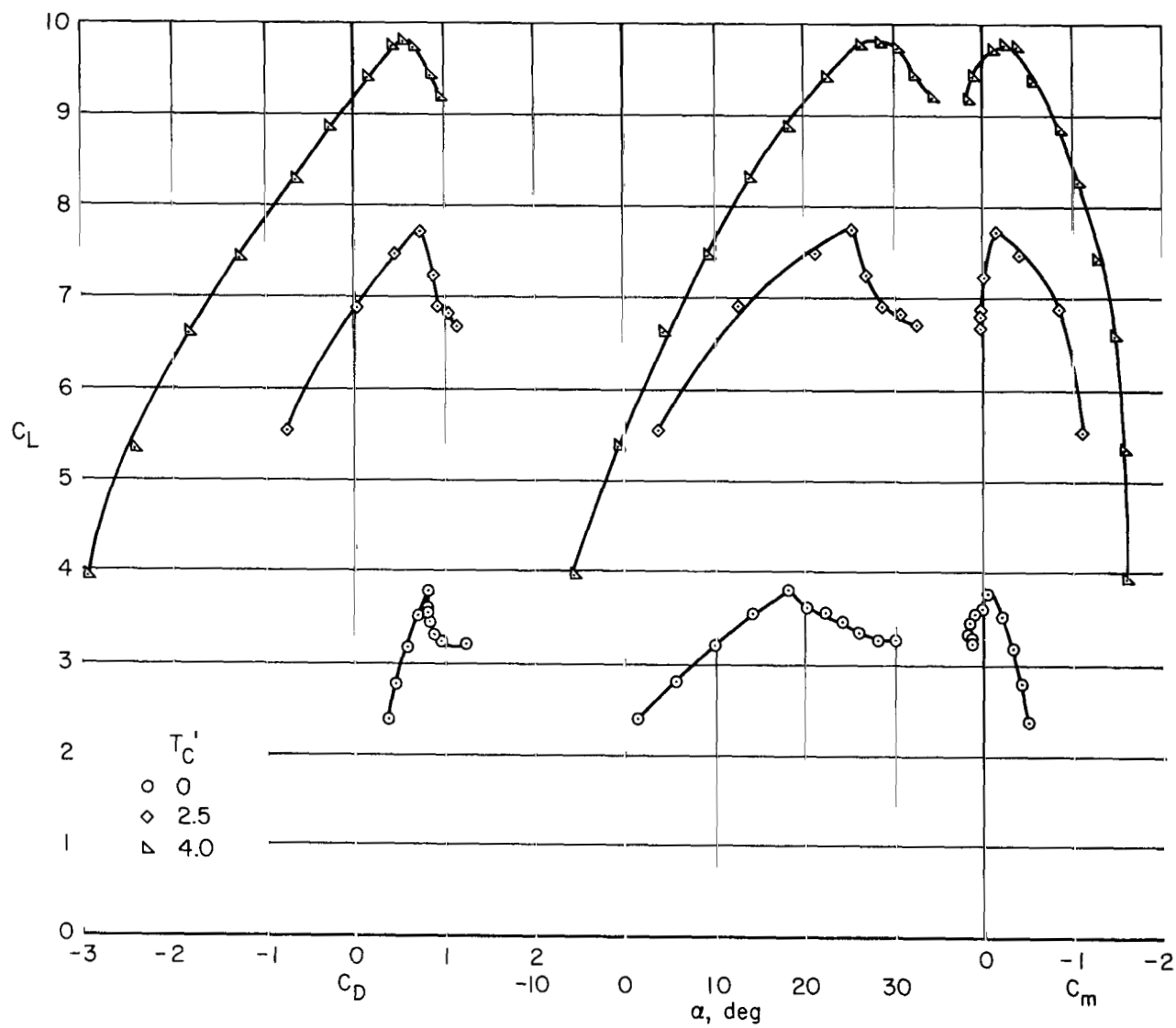(c) $\delta_f = 80°$, clean leading edge, $\beta_I = 16°$, $\beta_0 = 0°$.

Figure 13.- Continued.
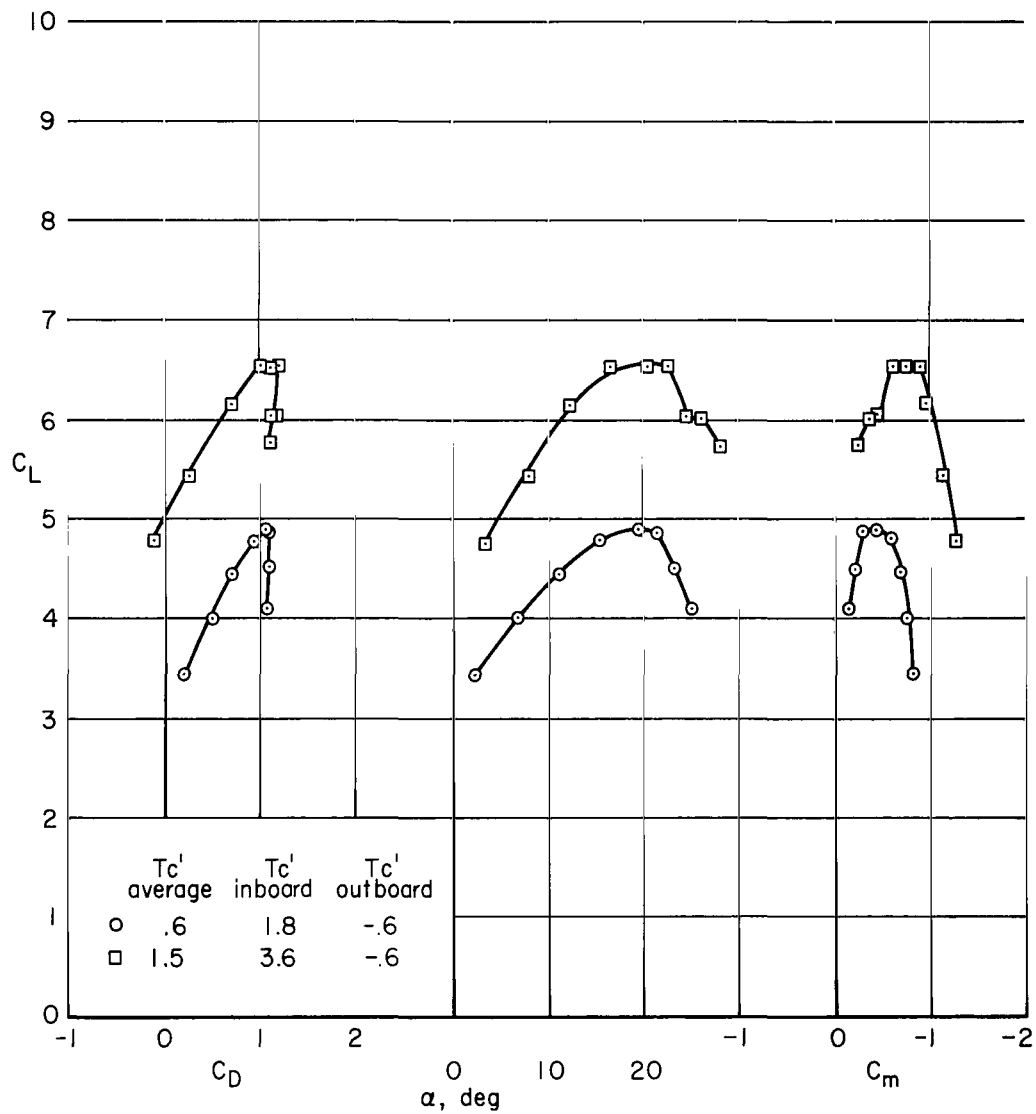
(d) $\delta_f = 80°$, full-span slats, $\beta_I = 16°$, $\beta_O = 0°$.

Figure 13.- Continued.

(e) δ_f = 100/60, full-span slats.

Figure 13.- Continued.

	Tc' average	Tc' inboard	Tc' outboard
○	.6	1.8	-.6
□	1.5	3.6	-.6

(f) δ_f = 100/60, full-span slats, β_I = 16°, β_0 = 0°.

Figure 13.- Concluded.

04U 0J1 27   ol 3Uo   68059   00J0 3
AIR FIRCE WEAPONS LABORATORY/AFWL/
KIRTLAND AIR FORCE BASE, NEW MEXICO 87117

ATT MISS MADELINE F CANOVA, CHIEF TECHNICAL
LIBRARY /WLIL/

"The aeronautical and space activities of the United States shall be conducted so as to contribute . . . to the expansion of human knowledge of phenomena in the atmosphere and space. The Administration shall provide for the widest practicable and appropriate dissemination of information concerning its activities and the results thereof."

—NATIONAL AERONAUTICS AND SPACE ACT OF 1958

NASA SCIENTIFIC AND TECHNICAL PUBLICATIONS

TECHNICAL REPORTS: Scientific and technical information considered important, complete, and a lasting contribution to existing knowledge.

TECHNICAL NOTES: Information less broad in scope but nevertheless of importance as a contribution to existing knowledge.

TECHNICAL MEMORANDUMS: Information receiving limited distribution because of preliminary data, security classification, or other reasons.

CONTRACTOR REPORTS: Scientific and technical information generated under a NASA contract or grant and considered an important contribution to existing knowledge.

TECHNICAL TRANSLATIONS: Information published in a foreign language considered to merit NASA distribution in English.

SPECIAL PUBLICATIONS: Information derived from or of value to NASA activities. Publications include conference proceedings, monographs, data compilations, handbooks, sourcebooks, and special bibliographies.

TECHNOLOGY UTILIZATION PUBLICATIONS: Information on technology used by NASA that may be of particular interest in commercial and other non-aerospace applications. Publications include Tech Briefs, Technology Utilization Reports and Notes, and Technology Surveys.

Details on the availability of these publications may be obtained from:

SCIENTIFIC AND TECHNICAL INFORMATION DIVISION

NATIONAL AERONAUTICS AND SPACE ADMINISTRATION

Washington, D.C. 20546